Spring 2015

Experimental and computational analysis of thermosyphon based water heaters

Siddarth Ashokkumar

Department:

EXPERIMENTAL AND COMPUTATIONAL ANALYSIS OF THERMOSYPHON BASED WATER HEATERS

by

SIDDARTH ASHOKKUMAR

A THESIS

Presented to the Graduate Faculty of the

MISSOURI UNIVERSITY OF SCIENCE AND TECHNOLOGY

In Partial Fulfillment of the Requirements for the Degree

MASTER OF SCIENCE

in

MECHANICAL ENGINEERING

2015

Approved by

Dr. Kelly Homan, Advisor
Dr. Ashok Midha
Dr. Edward Kinzel

ABSTRACT

Storage type electric water heaters are one of the most commonly found type of heaters in households today. Due to energy costs and limited generation capacity, there is a need for improving the efficiency of such water heaters. The efficiency of water heating systems have impact both at the household and at the national level, because of their sheer numbers. Efficient water heaters lead to lower utility bills for the consumer and also reduced demand on the grid supplying electrical power to such households. This leads to a reduction in the amount of fuel used in generating electrical power and potentially, greater reliance on more efficient baseload generating capacity. This thesis, investigates the performance of a novel storage type water heater with electric resistance heating elements and quantifies improvements to the First Hour Rating at no loss of Energy Factor. The modified storage type water heater utilizes an internal thermosyphon assembly to avoid large scale internal thermal mixing. First Hour Rating and Energy Factor Rating have been measured for a system configured in the conventional form and in the thermosyphon form. The introduction of a thermosyphon assembly into the storage volume significantly improves the First Hour Rating, by an amount equal to nearly 20%. Computational analysis of the thermosyphon tube is carried out using ANSYS FLUENT. The velocity profiles and skin friction coefficients are computed at different sections of the tube to identify the different flow regimes and pressure drops across the specific sections of the assembly.

ACKNOWLEDGMENTS

My research work has taken me through a very interesting journey in the last two years. A great deal of effort was put in to make sure the project was completed as per schedule. I certainly could not have done this all by myself. I would like to express my gratitude to Dr. Homan for trusting me with this interesting project. I still remember the day back in fall 2012, when I first met him, presenting my resume and talking about my past work experiences. Dr. Homan has been of immense support throughout this journey, guiding me towards the right path so as to complete this project in timely manner.

I thank the esteemed members of my graduate committee, Dr. Ashok Midha and Dr. Edward Kinzel for their support.

I would also like to thank the staff at the machine shop for putting up with my numerous requests for fabricating new parts for my experimental apparatus. I also thank Mr. Krishnan Raghavan for getting me upto speed with the use of MATLAB.

Lastly, I would like to express my gratitude to my parents Kovalavally Sudhama Ashokkumar, and Sheela Ashokkumar, and my sister Samyuktha Ashokkumar for supporting me over the last two years.

TABLE OF CONTENTS

Page

LIST OF ILLUSTRATIONS

LIST OF TABLES

NOMENCLATURE

Roman

C_f skin friction coefficient

C_p specific heat of the stored water, $(\bar{T}_{24} + \bar{T}_{su})/2$, Btu/lb°F kJ/kg°C

D diameter, in

k surface roughness height, in

L length, in

m meter

M_i mass withdrawn for the ith draw (i = 1 to 6), lb (kg)

$\dot{m}$ inlet mass flow rate to thermosyphon assembly

Q total energy used by the water heater during the 24-hour simulated use test including auxiliary energy such as pilot lights, pumps, fans, etc, Btu (kJ) (Electrical auxiliary energy shall be converted to thermal energy using the following conversion: 1kWh = 3412 Btu)

Q_{da} adjusted daily water heating energy consumption, Btu (kJ)

Q_{hr} hourly standby energy losses of the water heater, Btu/h (kJ/h)

Q_{stdby} total energy consumed by the water heater between the time at which the maximum mean tank temperature is observed after the sixth draw and the end of the 24-hour test period, BTU (kJ)

Re Reynolds number

s second

$\bar{T}_{24}$ mean tank temperature at the end of the 24- hour simulated use test, °F (°C)

$\bar{T}_{a,stby}$ overall average ambient temperature between the time when the maximum mean tank temperature is observed after the sixth draw and the end of 24 - hour simulated use test , °F (°C)

$\bar{T}_{a,stby,2}$ average ambient temperature during the total standby portion , $\tau_{stby,2}$, of the 24 hour test,°F (°C)

$\bar{T}_{del,i}$ average water outlet temperature measured during the ith draw (i=1 to 6), °F (°C)

$\bar{T}_{in,i}$ average water inlet temperature measured during the ith draw (i=1 to 6), °F (°C)

$\bar{T}_{o}$ mean tank temperature at the begining of the 24-hour simulated use test, recorded one minute before the first draw initiated, °F (°C)

$\bar{T}_{stby,2}$ mean tank temperature during the total standby portion , $\tau_{stby,2}$, of the 24- hour test,°F (°C).

$\bar{T}_{su}$ maximum mean tank temperature, observed after the sixth draw, °F (°C)

$\bar{T}_{t,stby}$ overall average storage tank temperature between the time when the maximum mean tank temperature is observed after the sixth draw and the end of 24 - hour simulated use test , °F (°C)

UA standby heat loss coefficient, Btu/h°F (kJ/kg°C)

V_{st} storage volume

Greek

ρ density of stored hot water, evaluated at $(\bar{T}_{24} + \bar{T}_{su})/2$, Btu/lb°F

η_r recovery efficiency

τ_{stdby} elapsed time between the time at which the maximum mean tank temperature is observed after the sixth draw and the end of 24-hour simulated use test, h

$\tau_{stby,2}$ number of hours during the 24 hour simulated test when water is not being withdrawn from the water heater

Subscripts

r restriction section

h heating section

s straightening section

1. INTRODUCTION

Water heaters are an essential appliance in every household today. Water heating accounts for nearly 15-20% of a home's energy use and on an average, about 64 gallons of hot water are used everyday in a domestic household. Taken together, this means that water heating has a significant impact on national energy use and utility grid profiles.

In today's market, several different types of water heaters in various capacities are available to the consumer. A first key distinction of such water heaters is the type of energy source used as input . Electric resistance, heat pump and gas water heaters represent the most common forms of electric and fossil-fueled sysetems. A second key distinction is based on whether the water heater has a storage capacity or is an instantaneous water heater. In spite of having such a wide variety of choices, storage type electric resistance water heaters remain the most popular form for domestic use due to their low cost and reliability. The storage capacity is essential since the performance requirements of a 3 gpm (Gallons Per Minute) flow at a water temperature rise of 24°C requires approximately six times the power provided by a 20 A current at 210 V, which is the typical requirement for a electric resistance storage type water heater. Heat pump water heaters can provide up to $300 per year in savings, however heat pump water heaters cost up to 5 times the price of an electric resistance water heater. Electric resistance storage type water heaters, due to their low cost and reliability, remain the most common type of water heater.

In electric resistance systems, the heating elements convert electrical energy unit-for-unit into heat energy which is transferred to the water in the storage volume. In such a system, there are only two broad sources of thermodynamic inefficiency. The most obvious loss is heat lost to the surrounding atmosphere through shell heat transfer. The second, less

obvious , loss mechanism is irreversibility internal to the system that is sassociated with internal thermal mixing between the incoming cold water and hot water generated at the heat transfer surface. Experiments conducted in the past show that storage type water heaters operate with a high degree of internal thermal mixing, resulting in reduced thermal performance of such heaters. Due to the ever rising demand for energy, energy cost and non-uniform utility demand profiles, a need for energy efficient water heaters exists. In the work described here, experimental and computational investigations was carried out on a residential scale water heater to determine its First Hour Rating and Energy Factor , along with the factors controlling it.

For the purpose of experimentation, an-off-the shelf electric storage water heating system was tested in both its conventional configuration and the novel, thermosyphon-based configuration. A thermosyphon utilizes buoyancy effects generated by a temperature gradient to circulate a fluid, acting like a weak pump. A thermosyphon tube can be categorized into open loop and closed loop geometries [Torrance, 1979]. In an open loop thermosyphon configuration, fluid that is delivered at the outlet of the tube is not recirculated back to the inlet. In a closed loop configuration, the fluid at the outlet of the thermosyphon tube is returned to the reservoir, from which the fluid is drawn into the thermosyphon tube. The thermosyphon tube assembly incorporated into the storage volume of the water heating system is of the latter type. Using industry-standard testing methods, the First Hour Rating and the Energy Factor of the water heater in the thermosyphon configuration was determined. A comprehensive comparison was made between the two configurations to enumerate the performance improvement of a thermosyphon tube based system over a conventional storage type water heater.

In addition numerical simulations of the thermosyphon assembly with nominal flow rates were conducted using ANSYS FLUENT to study the internal flow dynamics of the

thermosyphon tube assembly. Previous work by [McMenamy and Homan, 2006], showed that the outlet temperature of the fluid, from such thermosyphon tube assemblies is particularly sensitive to the overall flow restriction. Varying flow restrictions were simulated in FLUENT along with effects of varying surface roughness in the flow restriction. Skin friction coefficients and velocity profiles were plotted for the thermosyphon tube assembly and comparisons made to fully developed flow values. The pressure drop across the distinct sections of the assembly were computed to identify individual contributions to the overall losses.

2. LITERATURE REVIEW

Thermal stratification has long been recognized as central to desirable behavior of thermal energy storage devices. However, in systems which include simultaneous energy transfer, stratification is not easily accomplished or maintained. This is certainly true for storage type heaters. Neverthless, in a conventional storage type water heater, the transport dynamics within the storage volume have controlling impact on the quantity of hot water that can be drawn at a particular temperature. Previous investigations [McMenamy and Homan, 2006], have shown that in conventional systems only 80% of the storage volume is available at the minimum acceptable quality.

Numerous investigations have been carried out in attempts to determine the optimum design of electric water heaters so as to limit large scale mixing of the water in the storage volume with the incoming cold water. A dual tank water heater configuration, where the second tank had 25% of the total volume and 75% of the total power rating resulted in producution of more hot water at reduced energy consumption as described in [Kerim Kar and Kar, 1996]. Experiments have been carried out with different inlet and outlet configurations to determine, which configuration is best suited for the dynamic operation of the water heater. The experiment also helped determine the best inlet outlet configuration pair that gave the best thermal energy efficiencies [Fernández-Seara et al., 2007]. A horizontal wedge shaped inlet in the tank resulted in improved thermal stratification. This helped achieve higher discharge efficiency values. Better thermal stratification was also achieved by increasing aspect ratio and decreasing draw off rates as shown in [Hegazy and Diab, 2002]. Experiments have also been done comparing the wedge shaped inlet against slotted and perforated inlets. The experiments concluded that the slotted input

resulted in best thermal performance and was chosen as most suitable for efficient hotwater discharge [Hegazy, 2007].

The above investigations, have focussed only on throughflow-driven mixing controlled by inlet jet dynamics. The convntional wisdom is that mixing caused by energy addition, which results in a strong natural convection plume, is unavoidable. However work done by [McMenamy and Homan, 2006], focussed on studying the effects of implementing a thermosyphon loop inside a conventional resistance heating configuration. A laboratory scale model, made of uninsulated plexiglass enclosuse with a bottom inserted thermosyphon heating element was used. This work concluded that by isolating the energy addition surfaces, internal mixing caused by energy addition can be avoided, leading to better stratification and performance gains from such water heaters.

Numerical simulations carried out by [Benne and Homan, 2008], studied the coupling effect between a natural convection thermosyphon loop and a thermal storage device. Since a thermosyphon tube utilizes buoyance forces to circulate a fluid, continuous accumulation of energy in the storage volume, reduces the driving force and therefore affects the flow rate of the fluid through the thermosyphon tube assembly. It was found that a more uniform charge could be obtained with a transitional flow regime.

Numerical simulations by [Benne and Homan, 2009] also compared the performance of a stratified thermosyphon device and a fully mixed storage volume. It was determined that a higher rate of energy transfer is possible from the startified thermosyphon device when the dominant friction losses were targeted to the transitional regime.

The present work is based on the patented thermosyphon based electric resistance water heaters [Homan, 2006]. It explores the use of thermosyphon internals in a conventional off-the-shelf purchased residential scale storage type water heater. The effects on the transient performance of a conventional storage type resistance heater has been inves-

tigated by coupling such a thermosyphon tube assembly with the storage volume of the resistance heater. Further, numerical simulations using ANSYS FLUENT have been used to identify the sections of the thermosyphon tube, where flow losses are dominant. This is necessary for optimising the transient performance of the thermosyphon tube in a finite reservoir, such as the storage volume of the resistance heater.

3. EXPERIMENTAL PHASE

3.1. INTRODUCTION

First Hour and Energy Factor Ratings are the two industry-accepted means to measure the efficiency of a storage type water heater. Standardized test procedures have been developed by the United States Department of Energy (DOE) for determining the First Hour and Energy Factor Ratings. The test guidelines are detailed in volume 10 CFR Part 430 : "Test procedure for water heater; final rule". Laboratory tests as per the given guidelines have been carried out on a storage type water heater, with electric resistance heating. The heater has been tested in three different configurations viz. unmodified storage water heater, a modified system operated in conventional configuration and the modified system operated in thermosyphon configuration. For each of these configurations, First Hour and Energy Factor tests were conducted. Tests were carried out on the unmodified heater to first establish baseline results. The system was then modified so as to allow operation either in the conventional configuration or in a thermosyphon-based configuration. The modified heater was then operated without a thermosyphon assembly, to establish if changes to the heater shell affected the performance ratings. The heater was then operated with the thermosyphon assembly installed and tests conducted to quantify the performance gains.

3.2. EXPERIMENTAL SETUP

3.2.1. Conventional Electric Storage Water Heater. A conventional, off-the-shelf, 40 gallon storage type water heater with a nominal First hour Rating of 54 gallons was used. The standard configuration consists of two electric heating elements. One is sit-

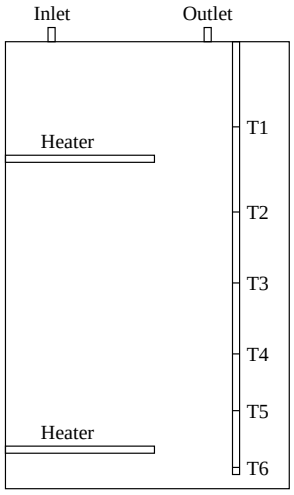

Figure 3.1. Conventional storage water heater configuration.

uated at a distance of 33 cm from the top surface of the water heater and a bottom element is located at a distance of 94 cm from the top surface of the water heater. The two heating elements are rated at 4.5 kW each. The watt transducer has an accuracy of 0.2% of the reading. The two heating elements operate in a sequence, one at a time. When starting from a cold start condition, the top heating element energizes and heats up roughly the top third of the storage volume. The bottom element is then energized to complete the heating process. Figure 3.1 shows the conventional storage water heater configuration.

3.2.2. System Modifications. Figure 3.2 shows the thermosyphon heater configuration. Modifications made to the conventional heater involves the use of a thermosyphon tube assembly. In the thermosyphon tube assembly, gravity acting on density differences causes fluid momentum generationand an ability to passively pump the fluid past the enclosed heating element. The thermosyphon tube assembly consists of a pipe, that is 1.5 inches in diameter and 45 inches in length. It is inserted into the heater through a centrally located hole at the top. A threaded coupling is welded to the top hole, which provides means for se-

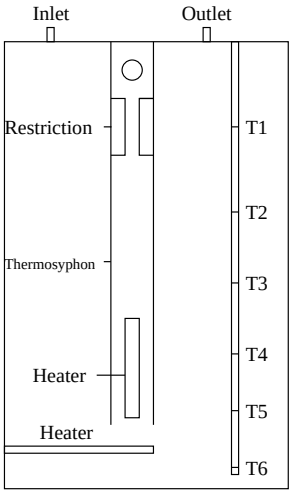

Figure 3.2. Thermosyphon water heater configuration.

curing the thermosyphon assembly at the top. The assembly is free hanging at the bottom. The top heating element is now placed in the lower portion of the thermosyphon assembly. The thermosyphon assembly draws water from the lower part of the heater, heats up the water and delivers the plume of hot water to the top. It does this to avoid large scale thermal mixing of the hot and cold water within the storage volume. The hot plume of water rises through the thermosyphon assembly and exits into the storage volume though slots drilled near the top of the tube.

3.2.3. Experimental Test Stand. Figure 3.3 shows the complete experimental test stand. The water heater is provided with type T thermocouples to measure internal tank temperatures, as illustrated in Figures 3.1 and 3.2. These thermocouples have an accuracy of $\pm 1^{\circ}$C (1.8°F). These thermocouples are mounted on the internal sacrifical anode. There are a total of six thermocouples located along the anode to determine internal tank temperatures at different heights inside the water heater. Thermocouples are also provided to measure the outlet water temperature and the ambient air temperature.

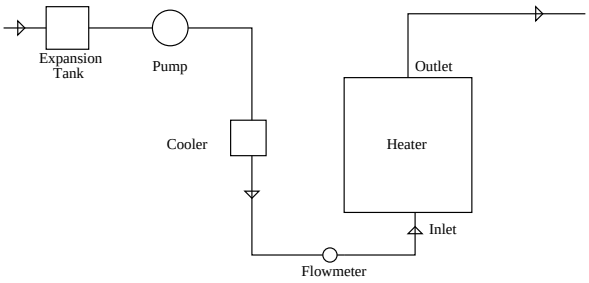

Figure 3.3. Experimental test stand.

The water heater is supplied with tap water, routed through a feed water pump to maintain desired flow rate. An expansion tank is also provided to compensate for the fluctuations in the pressure of the water supplied to the water heater. During draws, the hot water is drawn from the system at rate of 3.0 ± 0.25 gpm. This flow rate mentioned, is as per guidelines given in 10CFR Part 430. A Coriolis type flow meter with an accuracy of 0.5% of full scale (5 gpm)is used to measure the flow rate. The test procedure requires that, inlet water to the heater be supplied at $14.4 \pm 1.1\,^{\circ}$C. The building where the experimental setup is located provides service water at temperatures of 17 to 18°C. In order to bring down the water temperature to the required inlet temperature the inlet water is passed through a copper heat exchanger immersed in an ice bath.

Data aquisition is performed with the help of a LABVIEW program. The program records the internal tank temperatures, the inlet and the outlet water temperatures, as well as the ambient air temperatures. The flow rate of water is also measured. The raw data is stored as an excel file at the end of each experiment. The raw data generated by the

LABVIEW program is then processed by a user written MATLAB code, to determine the Energy Factor Rating, First Hour Rating and other quantities of interest.

3.3. DATA ANALYSIS

The experimental tests involved determination of First Hour Rating and Energy Factor on the unmodified and modifed system both with and without thermosyphon internals.

3.3.1. First Hour Rating. The First Hour Rating is the amount of hot water a fully charged heater can deliver in a one hour period, with the outlet water temperature maintained between $57.2 \pm 2.8\,^{\circ}$C and $43.3 \pm 2.8\,^{\circ}$C.

A First Hour Rating Test is started by initiating a draw of water after the tank has reached a maximum mean temperature of $57.2 \pm 2.8\,^{\circ}$C. During the draw the flow rate must be maintained at 3.0 ± 0.25 gpm. The time when the draw is initiated must be noted and the test terminated exactly sixty minutes later. The outlet temperature of the water is measured 15 seconds after initiating the draw which establishes the maximum outlet temperature for the draw. The inlet temperature of the water is maintained at $14.4 \pm 1.1\,^{\circ}$C. The initial hot water draw is terminated when the outlet water temperature drops reduces by $13.9\,^{\circ}$C. The volume of water pumped out during this first draw is then noted. Successive draws are initiated when the top thermostat of the water heater reaches its set point. At the end of sixty minutes, if a draw is occuring, it is allowed to continue until the outlet temperature reduces by $13.9\,^{\circ}$C. If a draw is not occuring, power to the heater is shut off, a draw is manually initiated and the outlet temperature of water from the heater is measured. If after thirty seconds, the outlet temperature form the water heater does not rise above the cut off temperature of the previous draw, the amount of water pumped out after an elapsed time of sixty minutes is not added to the total volume of water pumped out during the test. If the outlet water temperature is higher than the minimum outlet temperature of the previous

draw, the amount of water withdrawn is included in the total volume of water pumped out during the test. The total volume of water provided above the minimally-acceptable temperature constitutes the First Hour Rating of the water heater.

3.3.2. Energy Factor. The Energy Factor is intended as an approximation to the annual efficiency for the useful energy produced by the water heater. The Energy Factor determines the heater overall efficiency, based on the amount of hot water produced per unit of energy consumed per day. The energy factor is particularly sensitive to insulation level.

In order to determine the energy factor of the water heater, a total of 64.3 ± 1 gallons of water is removed in six equal draws. One-sixth of the total quantiy of water is pumped out in each draw. The average outlet temperature, $\bar{T}_{out}$ is to be maintained at $57.2 \pm 2.8\,^{\circ}$C. The inlet temperature, $\bar{T}_{in}$ is to be maintained at $14.4 \pm 1.1\,^{\circ}$C. The flow rate is to be maintained at 3.0 ± 0.25 gpm. Each draw of water is followed by a recovery period of the water heater. The energy consumed in each of the recovery periods is then used to calculate the energy factor of the water heater. Calculation of the energy factor was done based on the guideline given by DOE in 10 CFR Part 430. The formulas given below are used to determine the Energy factor of the water heaters. A MATLAB code was developed to automate the calculation of the Energy Factor of the water heater.

The energy factor, E_f, is computed as:

$$E_f = \sum_{i=1}^{6} \frac{M_i C_{pi} (135^{\circ}\mathrm{F} - 58^{\circ}\mathrm{F})}{Q_{dm}} \tag{3.1}$$

This quantity represents the ratio of the energy delivered by the water heater relative to the energy supplied to the water heater. The denominator, Q_{dm}, is the modified daily water

heating energy consumption. It is computed as the sum of

$$Q_{dm} = Q_{da} + Q_{HWD} \tag{3.2}$$

where Q_{da} is the adjusted daily water heating energy consumption. The second term, Q_{HWD} represents computation of the adjusted daily consumption. It takes into account that the temperature difference between the storage tank and surrounding ambient air may not be the nominal value of 67.5 °F(135 °F - 67.5 °F) or 37.5 °C (57.2 °C - 19.7 °C) due to the 10 °F (5.6 °C) allowable variation in storage tank temperature, 135 °F $\pm$ 5°F (57.2 °F $\pm$ 2.8°F), and the 5 °F (2.8 °C) allowable variation in surrounding ambient temperature 65 °F (18.3 °C) to 70 °F (21.1 °C). The adjusted daily water heating energy consumption is computed as:

$$Q_{da} = Q_D - [(\overline{T}_{stby,2} - \overline{T}_{a,stby,2}) - (135^{\circ}\text{F} - 67.5^{\circ}\text{F})]UA\tau_{stby,2} \tag{3.3}$$

$$Q_{da} = Q_D - [(\overline{T}_{stby,2} - \overline{T}_{a,stby,2}) - (57.2^{\circ}\text{C} - 19.7^{\circ}\text{C})]UA\tau_{stby,2} \tag{3.4}$$

A modification is also included for, when the temperature difference between the outlet water temperature and supply water temperature is not equal to the nominal value of 77°F. This value is computed as

$$Q_{HW} = \sum_{i=1}^{6} \frac{M_i C_{pi} (\overline{T}_{del,i} - \overline{T}_{in,i})}{\eta_r} \tag{3.5}$$

The energy required to heat the same quantity of water over a 77 °F (42.8 °C) temperature rise , Btu/day (kJ/day)is:

$$Q_{HW,77^\circ\mathrm{F}} = \sum_{i=1}^{6} \frac{M_i C_{pi}(135^\circ\mathrm{F} - 58^\circ\mathrm{F})}{\eta_r} \tag{3.6}$$

$$Q_{HW,42.8^\circ\mathrm{C}} = \sum_{i=1}^{6} \frac{M_i C_{pi}(57.2^\circ\mathrm{F} - 14.4^\circ\mathrm{F})}{\eta_r} \tag{3.7}$$

The difference between these two values is :

$$Q_{HWD} = Q_{HW,77^\circ\mathrm{F}} - Q_{HW} \tag{3.8}$$

$$Q_{HWD} = Q_{HW,42^\circ\mathrm{F}} - Q_{HW} \tag{3.9}$$

which must be added to the adjusted daily water heating energy consumption value. Thus, the daily energy consumption value, takes into account the temperature difference between the storage tank and ambient temperature may not be 67.5°F (37.5°C) and that the temperature rise across the storage tank may not be 77 °F (42.8 °C) is: $Q_{dm} = Q_{da} + Q_{HwD}$.

Finally, Q_d is the daily water heating energy consumption when the temperature difference between the storage tank ad surrounding ambient air is at the nominal value of 67.5°F.

$$Q_d = Q - \frac{V_{st}\rho C_p(\bar{T}_{24} - \bar{T}_0)}{\eta_r} \tag{3.10}$$

3.4. RESULTS AND DISCUSSIONS

First Hour and Energy Factor Ratings have been measured for the unmodified conventional storage water heater, the modified water heater operating in the conventional configuration and the modified water heater in thermosyphon configuration. The First Hour and Energy Factor Ratings mentioned in this section for each of the heater configuration is the average value obtained from carrying out three tests. The values measured for the First Hour Rating measured during the tests have a difference of $\pm$ 0.5 gallons from the average measured First Hour Rating in each of the configuration. There was no difference in the measured Energy Factor during the multiple tests conducted. A comprehensive comparison of the measured results is carried out to determine quantitatively the advantage of using a thermosyphon assembly inside the storage volume of a conventional water heater.

3.4.1. Unmodified Storage Water Heater System. The First Hour Rating test was carried out to verify the First hour Rating of a 40 gallon unmodified water heater. The upper thermostat is set for a temperature of $50 \pm 2.8\,^{\circ}$C. The vertical position of the upper thermostat corresponds approximately to the same position as that of thermocouple number 2. The Bottom thermostat is set to a temperature of $55 \pm 2.8\,^{\circ}$C. The upper thermostat is set at a lower temperature temperature to prevent over heating of the water above thermocouple number 2.

A draw of water is initiated and the time when the draw is initiated is noted. The outlet water temperature is measured with the help of the thermocouple mounted on the outlet water pipe as shown in Figure 3.4 . As per the test procedures, laid down by DOE in 10CFR Part 430, termination of the hot water draw occurs when the outlet temperature decreases by $13.9 \pm 2.8\,^{\circ}$C.

The internal tank temperatures shown in Figure 3.5 give a clear picture of the entire charging-discharging process. During the discharging process, the internal temperatures

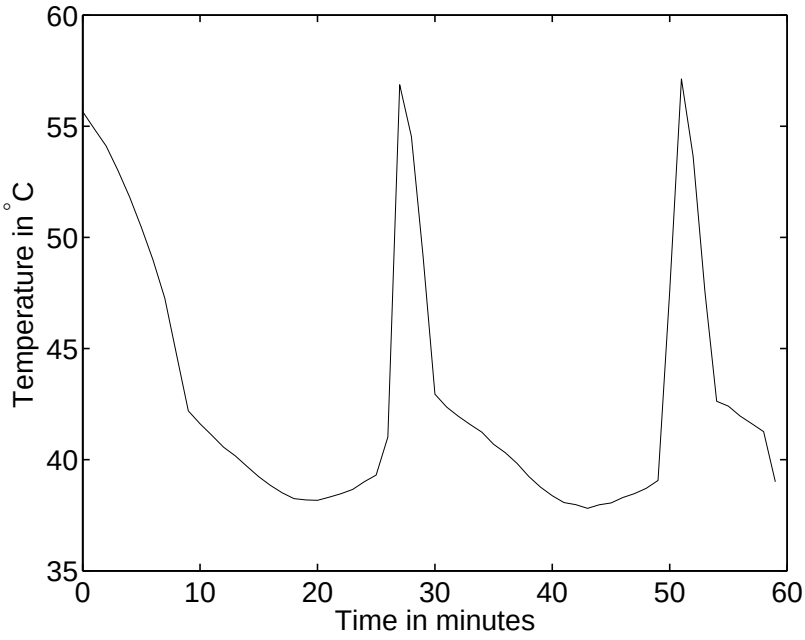

Figure 3.4. Dimensional outlet water temperature measured during a First Hour Rating Test of a 40 gallon unmodified water heater during. The highest outlet water temperature measured during each draw can be seen in the graph. The draw of water terminates when the outlet water temperature drops by 13.9°C. The test therefore had 3 separate discharges that sequences within the 60 minute test.

fall due to the fact that the hot water inside the tank is being used and the volume of used hot water is being replaced by cold water coming in from the bottom of the water heater. For this reason thermocouples 4, 5 and 6 show a rapid reduction in temperature almost as soon as the draw is initiated. During the charging process, the thermocouples show an increase in temperature. Thermocouples 1 and 2 are of particular interest here as they show the maximum rise in temperature. Initially during the draw, the bottom thermostat senses a drop in temperature due to the incoming cold water. The bottom thermostat becomes unsatisfied causing the bottom heating element to energize. As the draw continues, the cold water entering the water heater fills up the heater and causes the top thermostat to become

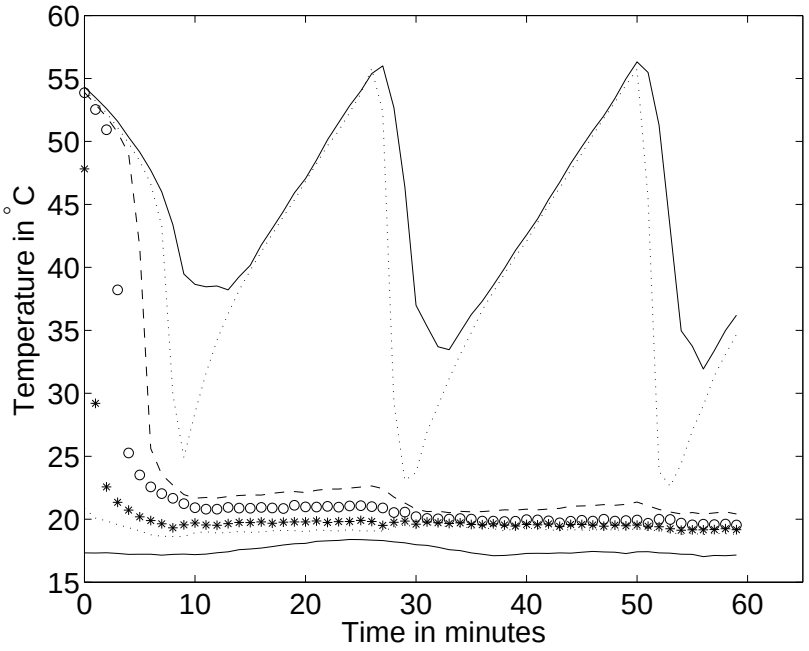

Figure 3.5. Dimensional internal tank temperatures shown for an unmodified 40 gallon water heater during a First Hour Rating test. Discharging and subsequent charging periods of the water heater can be seen from the fall and rise in the internal tank temperature.

unsatisfied. Once the top thermostat drops below its setpoint, the top heating element is energized and the bottom heating element cuts out.

A plot of cumulative volume withdrawn, shown in Figure 3.6 , indicates that successive draws are shorter compared to the first draw. The Test procedures, laid down in 10CFR part 430 requires that successive draws be initiated when the heating element involved in the successive charging process, in this case the top heating element cuts off due to the thermostat being satisfied. As seen in Figure 3.5, this happens when the average tank temperature is lower than the average tank temperature prior to the first draw. As a result, the outlet temperature drops faster as compared to the first draw resulting in shorter successive draws. For the specific test illustrated, three valid draws shown in Figure 3.5

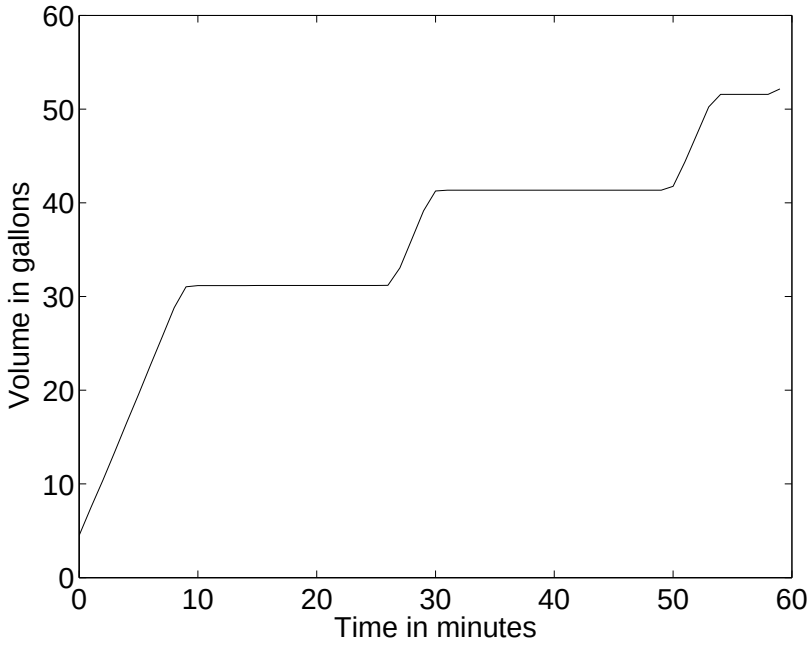

Figure 3.6. Dimensional volume of water pumped out during a First Hour Rating test of an unmodified 40 gallon water heater.

occured. No valid draws were made after the elapsed time of 60 minutes. Table 3.1 gives the volume of water recorded for each draw for the different water heater configurations.

In the Energy Factor test, a total of six draws were made during the test. Figure 3.7 shows the instantaneous power input to the heater. When a draw is made, the bottom thermostat becomes unsatisfied first and the lower heating element is energized. During the entire recovery period, only the bottom heating element is energized. This is because only about 10.7 gallons are withdrawn each draw and such small draws do not cause the top thermostat to become unsatisfied and the top heating element to energize. This can also be seen from Figure 3.8 showing the internal tank temperatures. The top three Thermocouples, labeled 1,2 and 3, do not show an appreciable drop in temperature when the draw is made, only the bottom thermocouples show a decrease thereby making the lower thermo-

Table 3.1. Dimensional volume of water pumped out in gallons during each draw in the First Hour Rating test.

Configuration	One	Two	Three	Four
Unmodified	31.1	10.1	10.2	-
Modified without thermosyphon	30.6	10.0	10.1	-
With thermosyphon	33.5	10.2	10.9	9.0

stat unsatisfied and energizing the lower heating element. It is also seen that the heating element is energized twice for shorter periods during standby. This is done by the heater to take care of a fall in internal temperatures during the standby period. The energy factor of the water heater was calculated using a MATLAB code.

3.4.2. Modified Water Heater in Conventional Configuration. The modified water heater, with the centrally located opening on the top, was first operated in the conventional configuration. The additional top opening was plugged and the two heating elements placed in their usual locations. The water heater was operated without the thermosyphon assembly. The First Hour and Energy Factor tests were conducted and the results were compared against baseline results generated from the conventional unmodified water heater. This comparison is important to establish whether modifications to the water heater affect the First Hour and Energy Factor rating of the water heater. Figure 3.9 shows the internal tank temperature profiles when the modified water heater is operated in the conventional configuration. The modified water heater, operating in the conventional configuration, has similar internal tank temperature profiles as the conventional configuration. Figure 3.10 shows the volume of water pumped out during the First Hour Rating test. The volume of water pumped out in each draw is similar to the unmodified water heater. The small differences in the values observed can be attributed to minor differences in experimental

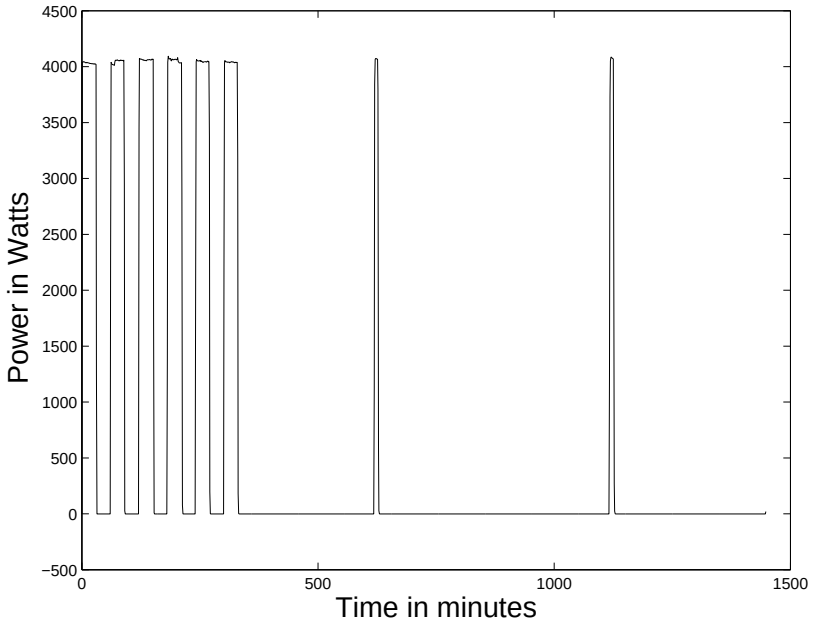

Figure 3.7. Dimensional instantaneous power input to the unmodified 40 gallon water heater during the simulated 24 hour Energy Factor test.

conditions, such as inlet water temperature, ambient temperature etc. Table 3.1 shows the volume of water pumped out in each draw during the First Hour Rating test. The conclusion is that the modified water heater operating in the conventional configuration behaves almost identical to the unmodified water heater.

Energy Factor tests were also carried out on the modified water heaters, again without installing the thermosyphon assembly. The primary purpose of these tests was to determine, if the added port created a change in the Energy Factor Rating of the water heater. The First Hour Rating tests indicated that, the centrally located hole did not cause any change to the First Hour Rating. Figure 3.11 and 3.12 show the instantaneous power input and the tank temperatures of the water modified water heater. These appear very similar to those plotted for the unmodified water heaters. The energy factor calculated for the

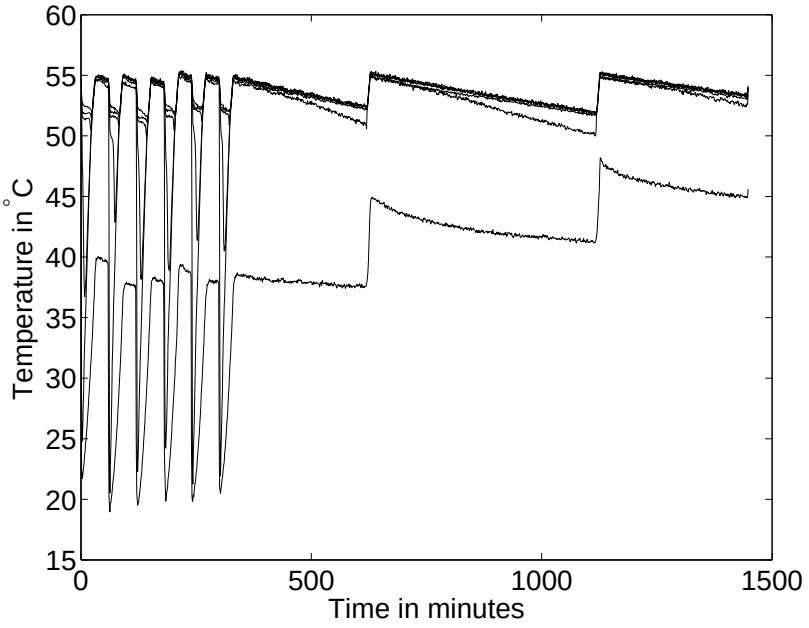

Figure 3.8. Dimensional internal tank temperatures for an unmodified 40 gallon water heater plotted against time during the simulated 24 hour Energy Factor test. Discharging and subsequent charging periods of the water heater can be seen from the fall and rise in the internal tank temperature.

modified water heater was similar to the unmodified water heater as shown in Table 3.2

3.4.3. Modified Water Heater in Thermosyphon Configuration. Finally the same First Hour Rating test procedures were followed for the water heater with the thermosyphon assembly installed. The water heater was first filled with cold water and then the elements were energized in sequence. The first element to energize is the heating element inside the thermosyphon assembly.

The initial charging process from a cold initial condition shows significant differences as compared to the conventional configuration. The heating element to start the charging process is the element inside the thermosyphon assembly. This results in a plume of hot water rising up the thermosyphon assembly and entering into the storage volume

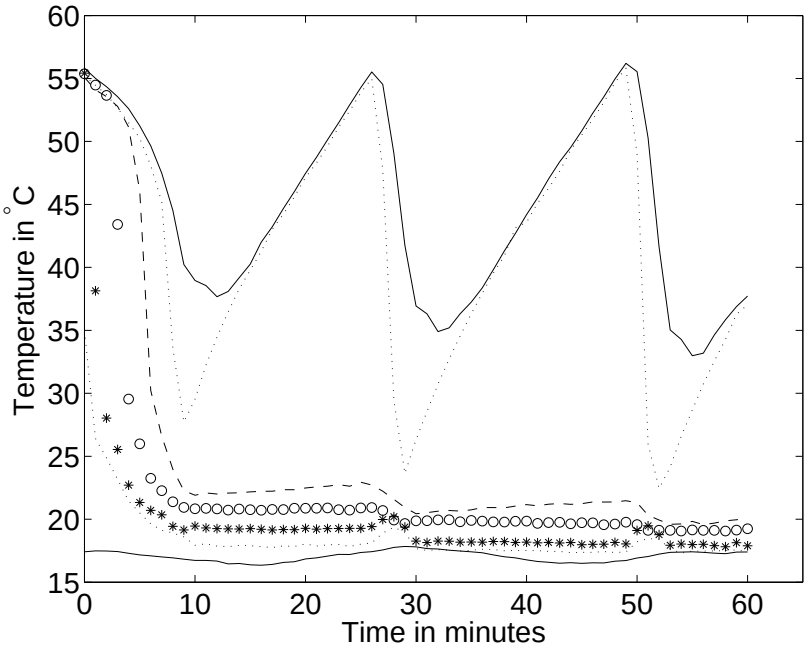

Figure 3.9. Dimensional internal tank temperatures shown for modified 40 gallon water heater, operated in the conventional configuration during a First Hour Rating test. Discharging and subsequent charging periods of the water heater can be seen from the fall and rise in the internal tank temperature.

through the exit ports at the top. Due to this process happening the top thermocouple shows a rapid increase in temperature. With appropriate flow restriction it can be seen that the thermocouple shows a rapid rise in temperature up to 53°C before slowing down. Figure 3.13 shows the internal tank temperatures during the charging and the discharging periods. Notably the other thermocouples do not show any appreciable change during this period. Once the top thermocouple reaches 53°C, its rise in temperature slows down and thermocouple 2 starts to show an increase in temperature. This is because of the continous heating provided by the heating element in the thermosyphon assembly and the cold water in the storage volume being replaced by the hot plume of water exiting the thermosyphon assembly and entering into the storage volume. A natural convection loop is set up in-

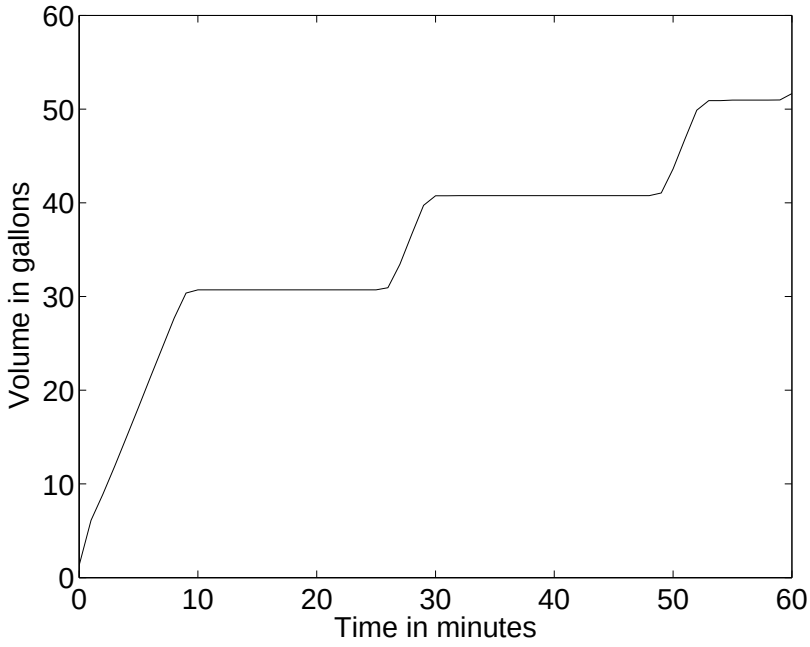

Figure 3.10. Dimensional volume of water pumped out during a First Hour Rating test of an modified 40 gallon water heater, operated in the conventional configuration.

side the heater storage volume and as the hot and cold water interface moves towards the bottom, the driving power of this natural convection loop reduces. The top thermostat settings was reduced to 47 °C so as to avoid over heating the water to beyond the acceptable limit in the space above the top thermocouple. It can also be seen from Figure 3.13, that thermocouples 2 and 3 show a rise in temperature before the heating element inside the thermosyphon deenergizes.

Also evident in Figure 3.13, is the fact that the thermosyphon based assembly has a shorter charging period, which resulted in 3 charging periods as compared to only 2 charging periods with the unmodified water heater. Figure 3.14 shows the total volume of water pumped out. The first draw is larger than the first draw of the unmodified water heater. The reason for the increase in the first draw is because with the modified water heater,

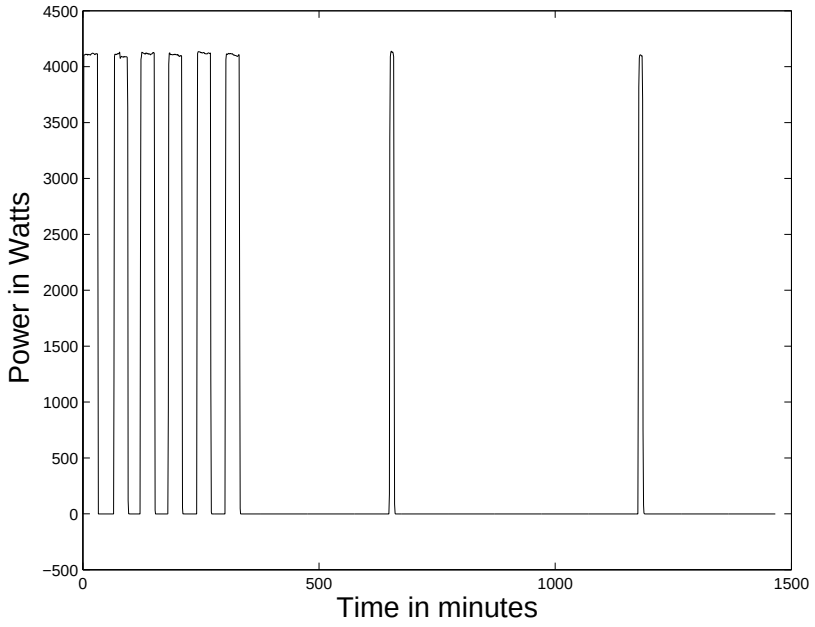

Figure 3.11. Dimensional instantaneous power input to the 40 gallon water heater during the simulated 24 hour Energy Factor Test. The water heater was modified to accomodate the thermosyphon assembly. During this test the water heater was operated without a thermosyhon.

when the bottom thermostat first gets unsatisfied during the discharge process, control is transferred to the the heating element inside the thermosyphon assembly. Hot water plumes are continuously discharged into the storage volume of the water heater. From the graph showing the internal temperatures in Figure 3.14, it is clearly seen that the thermocouples show a gradual decrease in temperature as compared to the unmodified water heater. This results in a longer first discharge, which in turn results in a larger volume of water being pumped out during the first draw.

With the modified water heater Figure 3.14 shows that, four valid draws are made as compared to the 3 draws made with the unmodified water heater. In the modifed water heater the last valid draw is made after the elapsed time of 60 minutes. The draw is counted

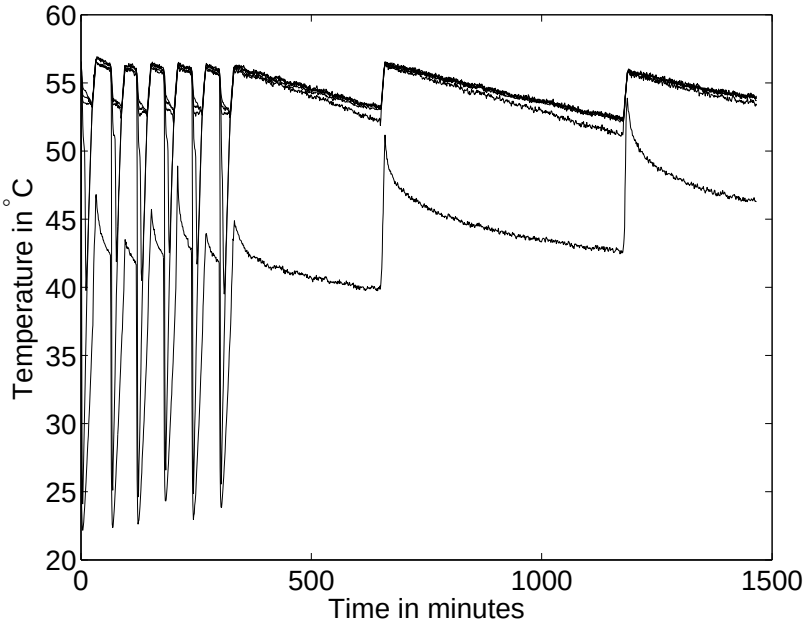

Figure 3.12. Dimensional internal tank temperatures for a modified 40 gallon water heater operated without a thermosyphon assembly plotted against time during the simulated 24 hour Energy Factor test. Discharging and subsequent charging periods of the water heater can be seen from the fall and rise in the internal tank temperature.The water heater was modified to accomodate a thermosyphon assembly. During this test the water heater was operated without a thermosyphon.

as a valid draw, since the outlet temperature of the water, when the discharge was made, was higher than the previous draws cut off temperature. A major portion of the difference between the FHR of the modified and unmodified water heater is accounted for in this final draw. A total of 9.0 gallons were pumped out during this draw. The plot showing the outlet temperature of water that the fourth draw is a valid draw. The maximum outlet temperature for the fourth draw is $57.2 \pm 2.8\,^{\circ}\mathrm{C}$, which is higher than the cut off temperature of the previous draw. Table 3.2 shows the First Hour Rating and the Energy Factor Rating of the water heater in the three different configurations. The modified water heater with the thermosyphon assembly, has an increased First Hour Rating.

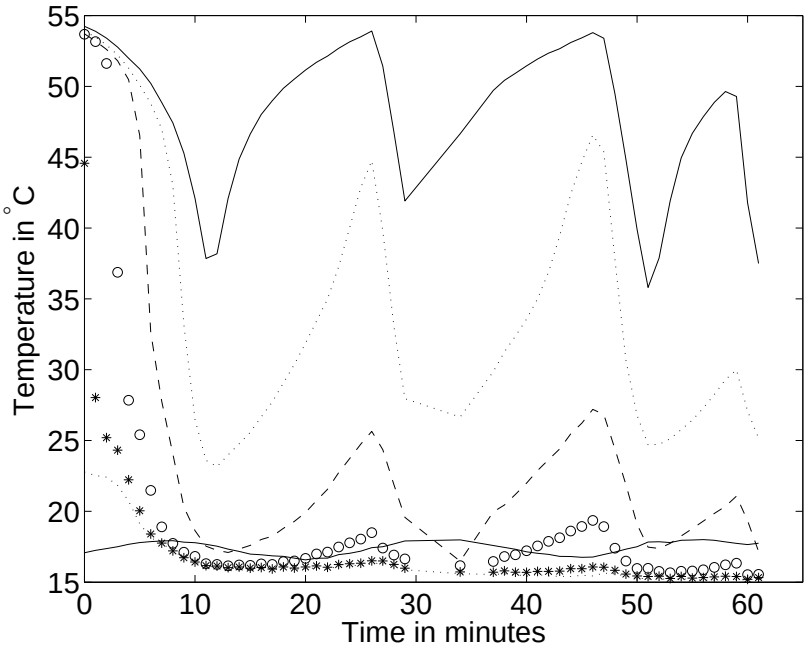

Figure 3.13. Dimensional internal tank temperatures plotted against time for 40 gallon modified water heater operated with a thermosyphon assembly installed during a First Hour Rating test. Charging and discharging periods of the water heater can be seen from the rise and fall in the internal tank temperature.

Energy factor tests were also conducted with the water heater run in the thermosyphon configuration. The energy factor test was conducted in accordance to the test procedures laid down in 10CFR Part 430. The water heater was filled with cold water and then the heating elements were energized in sequence starting with the heating element in the thermosyphon assembly.

The Energy Factor test requires six equal draws of 10.7 gallons. This small amount of water only unsatisfies the bottom thermostat. The temperature profiles in Figure 3.15 indicate that the top 3 thermocouples do not show any significant drop in temperature. Figure 3.16 shows the instantaneous power input to the water heater. Only the bottom heating element can get energized as energizing the top heating element in such conditions

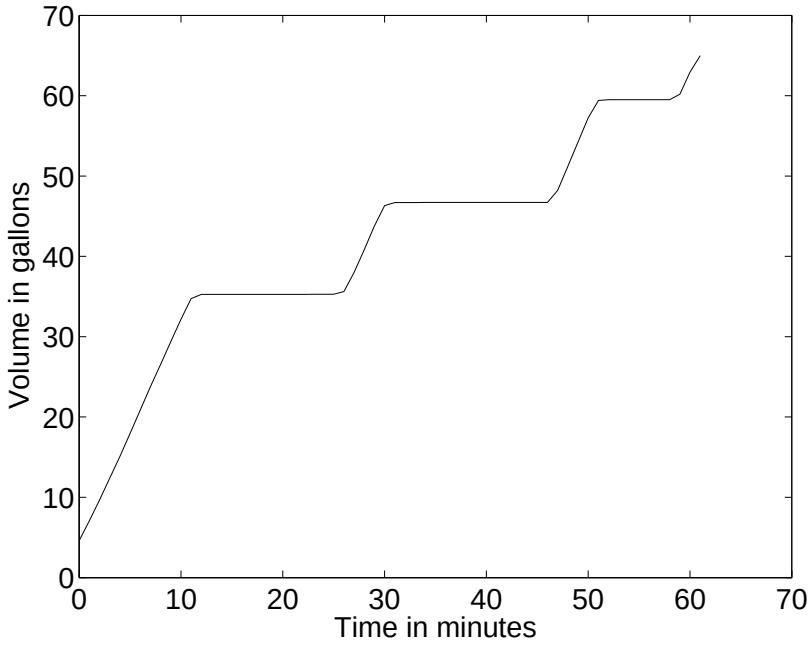

Figure 3.14. Dimensional volume of water pumped out plotted against time during a First Hour Rating test of a modified 40 gallon water heater operated with an installed thermosyphon assembly plotted against time.

will result in water temperatures beyond the necessary limit. Interestingly Figure 3.16 shows that the power input to the water heater in the thermosyphon configuration is very similar to the unmodified water heater. The energy factor is therefore insensitive to the different configurations as indicated in Table 3.2.

3.4.4. Conclusion. The First Hour Rating and Energy Factor Rating of a storage type water heater was recorded. Baseline tests were first conducted, to etablish that the standardized test procedures are being followed. The baseline tests yielded values similar to manufacturer claimed values. It is seen that a modified water heater operating without a thermosyphon, behaves similar to the water heater in a conventional configuration. The First Hour and Energy Factor Ratings obtained are similar to the values obtained from

Table 3.2. First Hour Rating and Energy Factor of a 40 gallon water heater in the three different configurations. The values measured for the First Hour Rating during the tests have a difference of $\pm$ 0.5 gallons from the average measured First Hour Rating in each of the configuration, while the values for the Energy was close to the average measured value of 0.89

Configuration	FHR	EF
Unmodified water heater	51.5	0.89
Modified water heater without thermosyphon	50.9	0.89
With thermosyphon	63.7	0.89

the conventional configuration. Addition of a thermosyphon assembly to the water heater resulted in significant performanc gains. The thermosyphon assembly helped achieve better stratification, which improved the First Hour Rating of the water heater. Increments of up to 10 gallons have been achieved with the thermosyphon configuration. It is also noted that the Energy Factor Rating of the water heater remains unchanged in all the three configurations. Therefore, the addition of a thermosyphon assembly provides significant improvement in thermal performance of the water heater.

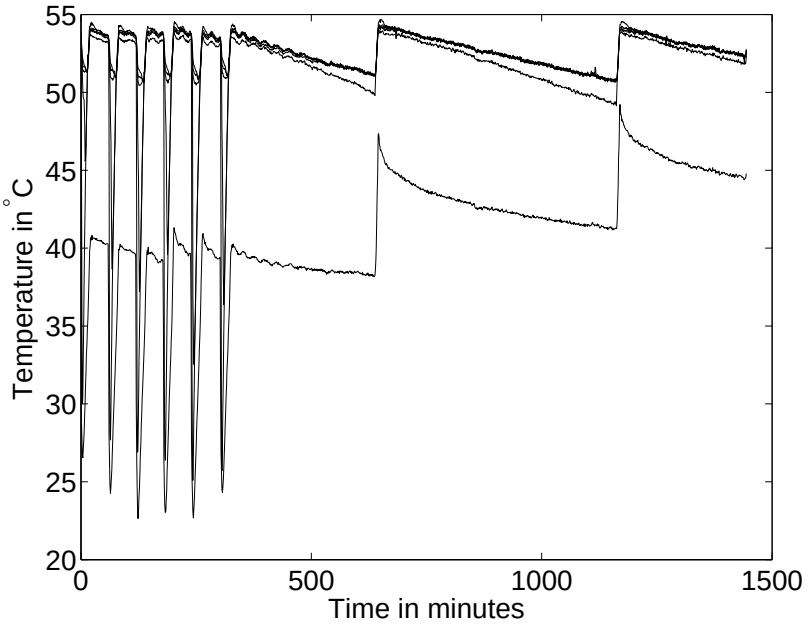

Figure 3.15. Dimensional internal tank temperatures plotted against time for a modified 40 gallon water heater operated with a thermosyphon assembly during the simulated 24 hour Energy Factor test. Discharging and subsequent charging periods of the water heater can be seen from the fall and rise in the internal tank temperature.

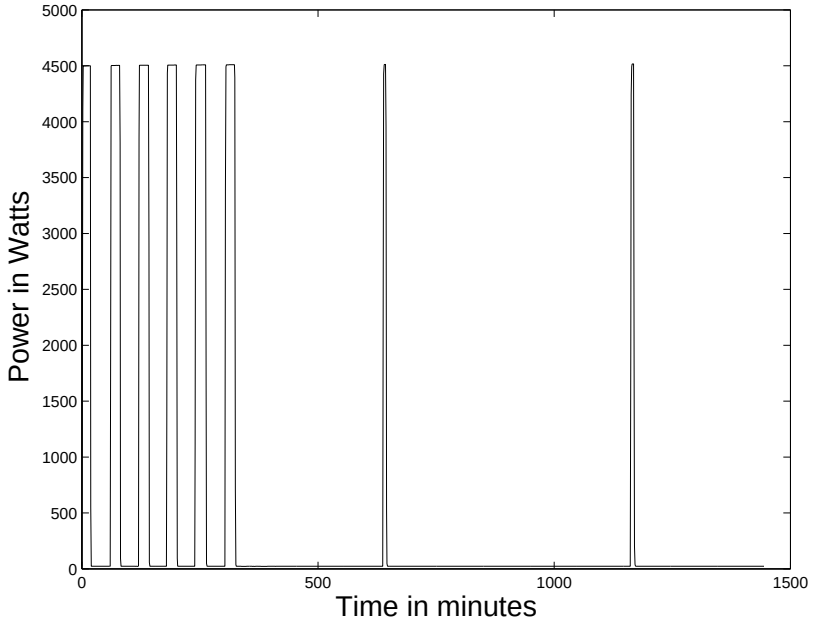

Figure 3.16. Dimensional instantaneous power input to the modified 40 gallon water heater operated with a thermosyphon assembly during the simulated 24 hour Energy Factor test.

4. COMPUTATIONAL PHASE

4.1. PROBLEM SETUP IN FLUENT

It is important to design the thermosyphon assembly such that a nominally constant temperature within acceptable limits, is available at the thermosyphon outlet. Understanding internal flow dynamics is essential in achieving the optimal thermosyphon design. The outlet temperature from the thermosyphon assembly is largely dependent on the flow restriction diameter placed inside the thermosyphon assembly as shown by [McMenamy and Homan, 2006]. As a first step in the design of a thermosyphon assembly, 2D numerical simulations of a simplified thermosyphon assembly have been carried out using ANSYS FLUENT, to study the internal flow dynamics. Varying flow restriction diameters have been simulated in ANSYS FLUENT, as it is a crucial component in dictating the performance of the thermosyphon assembly. The effects of varying the surface roughness of the flow restriction has also been studied. In order to analyse the internal flow dynamics, skin friction coefficients and velocity profiles have been plotted for the thermosyphon assembly and quantitative comparisons have been made to fully developed flow values. In an optimal design of the thermosyphon assembly, it is desirable to achieve the dominant pressure loss across the flow restriction element. The pressure drops across the different sections of the thermosyphon assembly has been computed to understand how multi dimensionality affects the pressure drop.

4.1.1. Thermosyphon Geometry. The tube geometry is drawn using the Design Modeler in ANSYS FLUENT. The thermosyphon assembly is divided into three distinct sections: heater, straightening and flow restriction sections. Figure 4.1 illustrates the different sections of the thermosyphon tube geometry. The total length of the thermosyphon

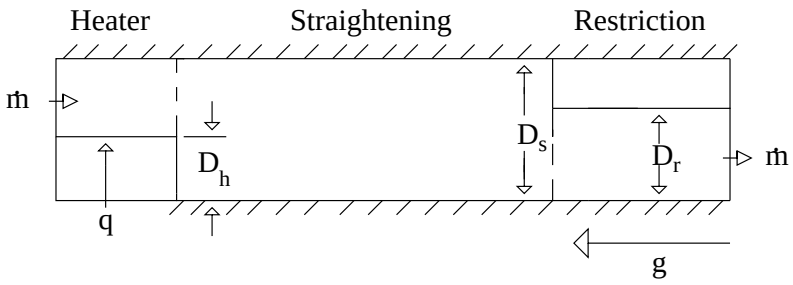

Figure 4.1. The thermposyphon geometry divided into heater, straightening and flow restriction section. Gravity is acting in the downward direction as shown in the picture.

tube is L=49 inches. The inner diameter of the tube is $D_s = 1.5$ inches in the straightening section. The length and diameter of the thermosyphon assembly matches the dimensions of the experimental thermosyphon assembly. The diameter of the thermoyphon tube geometry in the flow restriction section is denoted by D_r and is varied between 0.5 inch, 0.375 inch and 0.625 inch respectively. Three different types of heater configurations have been considered in the thermosyphon assembly. Figures 4.2 , 4.3 , and 4.4 show the different heater geometries simulated in ANSYS FLUENT. The cylindrical heater has a length $L_h = 7.25$ inches and a diameter $D_h = 1.375$ inches. An alternate cylindrical heater with a length $L_h = 7.64$ inches and a diameter $D_h = 1.25$ inches. A toroidal heater with a total of nine heating rings, each of diameter $D_h = 0.3125$ inch as seen in 2D, spanning a length $L_h = 4.5$ inches. One half of the thermosyphon tube geometry was drawn in 2D in the design modeler to be simulated as an axisymmetric case. Each of the heaters have a fixed surface area of 30 in^2.

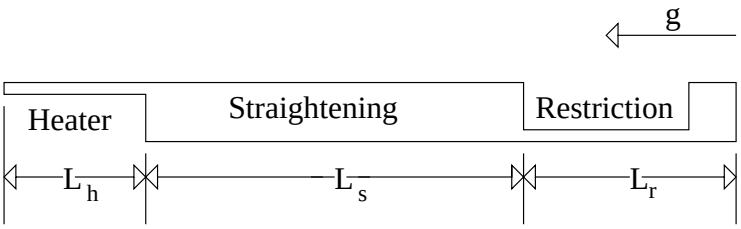

Figure 4.2. Cylindrical heater geometry simulated in ANSYS FLUENT. Gravity is acting in the downward direction. L_h is the length of the heating section, L_s is the length of the straightening section and L_r is the length of the restriction section. one half of the actual geometry is shown.

4.1.2. Boundary Conditions and Fluid Properties. The inlet boundary condition of the thermosyphon tube is set to a constant mass flow with a rate of $\dot{m} = 0.026$ kg/s for a low flow condition and $\dot{m} = 0.102$ kg/s for a high flow condition. The low flow condition is solved numerically using the molecular viscosity model (laminar) and the high flow condition is solved using the Standard k-ω turbulence model. Figure 4.5 shows the skin friction coefficients for simple pipe plotted at a flow velocity of 0.22 m/s. It is seen that the Standard k-ω model produces results closest to the molecular viscosity model. Hence the Standard k-ω model was chosen as the turbulence viscocity model. The fluid inflow temperature is fixed at 288 K. The outlet of the thermosyphon tube is set as a pressure outlet boundary condition. For the cylindrical heater, the outlet temperature from the thermosyphon at a mass flow rate of $\dot{m} = 0.026$ kg/s corresponds to 318 K. At a mass flow rate of $\dot{m} = 0.102$ kg/s, the outlet temperature is 313 K. For the alternate cylindrical heater,

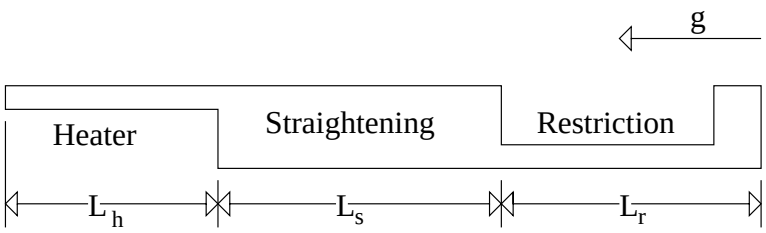

Figure 4.3. Alternate cylindrical heater geometry simulated in ANSYS FLUENT. Gravity is acting in the downward direction. L_h is the length of the heating section, L_s is the length of the straightening section and L_r is the length of the restriction section.one half of the actual geometry is shown.

the outlet temperature at $\dot{m} = 0.026$ kg/s is 349 K and at $\dot{m} = 0.102$ kg/s the outlet temperature is 317 K. With the toroidal heater, the outlet temperature from the thermosyphon tube is 347 K at $\dot{m} = 0.026$ kg/s and 310 K at $\dot{m} = 0.102$ kg/s. The heater has a constant heat flux of 236842 W/m^{2}K. The walls of the thermosyphon tube were taken as adiabatic. Variations in outlet temperature occur between different heater geometries due to the heat transfer regime being predominantly forced in the case of cylindrical and it being mixed in the toroidal heater.

The simulated fluid is water with a density of $\rho = 998.2$ kg/m^3. The impact of gravity on the flow field is modeled by the Boussinessq approximation. The specific heat is taken to be constant at $C_p = 4.182$ kJ/kgK. The thermal conductivity is set to k = 0.6 w/mK. The fluid has a viscocity of $\mu = 0.001003$ kg/m.s and the thermal expansion coefficient is set to 0.00347 1/K.

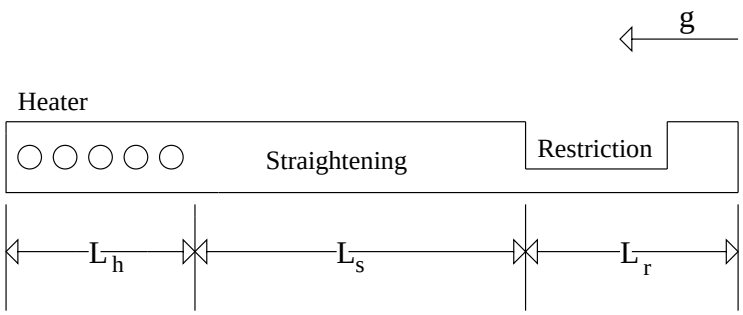

Figure 4.4. Toroidal heater geometry simulated in ANSYS FLUENT. Gravity is acting in the downward direction. L_h is the length of the heating section, L_s is the length of the straightening section and L_r is the length of the restriction section. one half of the actual geometry is shown.

The steady-state, pressure-based solver is used with gravity acting in the downward direction. The solver scheme is set to SIMPLE with a Least-squares cell-based gradient. The pressure gradient is set to body force weighted with the momentum and energy gradient set to second order upwind. Default under relaxation factors have been used and the residuals are set to 10^{-6}. Each simulation was initialized from the inlet boundary condition.

4.1.3. Meshing and Grid Convergence. High quality meshing of the thermosyphon tube geometry is critical to obtain accurate results from FLUENT simulation. The thermosyphon tube geometry was meshed using the meshing software available in ANSYS Workbench. The entire thermosyphon assembly was meshed using quadrilateral meshing elements.

A grid convergence study was carried out on the thermosyphon assembly with an integral heater, in which the heat flux was imparted to a portion of the thermosyphon assem-

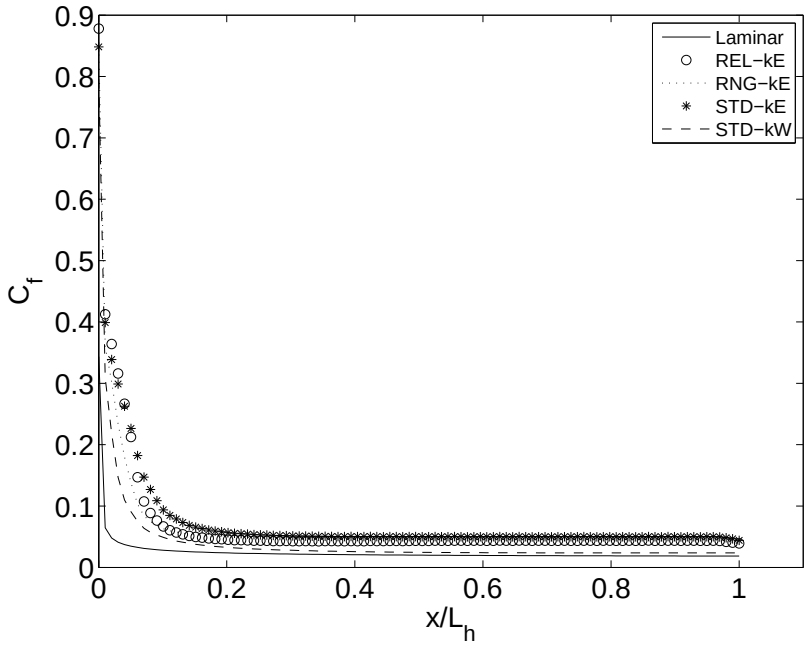

Figure 4.5. Skin friction coefficient plotted for a simple pipe with velocity inlet condition of 0.22 m/s. The skin friction coefficient of the Standard k-ω model comes closest to the molecular viscosity(laminar) model.

bly, to verify if the results obtained were mesh resolution independent. The thermosyphon tube geometry was simulated in FLUENT and the skin friction coefficient was plotted first for a mesh with 10000 elements. The same tube geometry was simulated with 25000 and 40000 elements and the skin friction coefficient was plotted for the straightening section of the thermosyphon assembly in each case. The length average skin friction coefficient was also computed analytically for the straightening section of the thermosyphon assembly. The results indicate no difference in the skin friction coefficients plotted for the 25000 element and the 40000 element mesh. Figure 4.6 shows the skin friction coefficients plotted for the thermosyphon tube geometry for a 10000, 25000 and 40000 element mesh. The skinfriction coefficient values plotted for the 25000 and 40000 element mesh overlap each

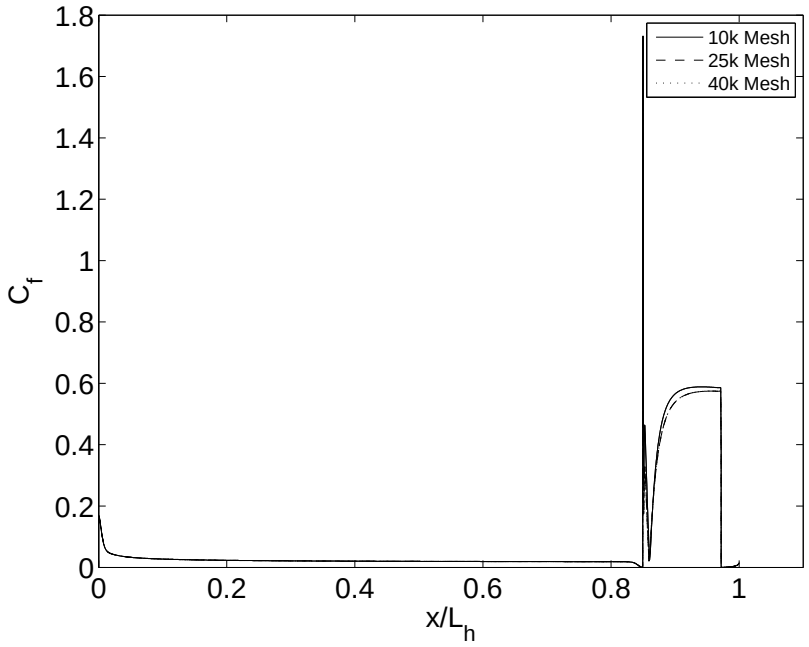

Figure 4.6. Skin friction coefficient plotted for the thermosyphon assembly using 10k, 25k and 40k element mesh for grid convergence study.

other. The value of skin friction coefficient using the 10000 element mesh is shown by the dotted line. The length averaged skin friction coefficient calculated analytically in the straightening section is $C_f = 0.014$, this matched with the length averaged skin friction coefficient values generated by the 25000 and 40000 element mesh.The length averaged skin friction coefficent for the 10000 element mesh is $C_f = 0.0179$. From the grid convergence results, a 25000 element mesh was selected for all further simulations.

4.2. RESULTS AND DISCUSSION

Steady state solutions are obtained for low- and high- flow conditions through the thermosyphon assembly. In the thermosyphon assembly, gravity acting on the temperature differences circulates the fluid through the thermosyphon tube, eliminating the need for a separate mechanical pump. The high and low-flow conditions correspond to conditions at the start of the charging process and closer to the end of the charging process. Under these conditions, the loop driving pressure is at its maximum and at its lowest value. Understanding flow dynamics inside the thermosyphon assembly is essential to being able to fully predict its behavior, since the assembly may contain portions of both laminar and turbulent flow regimes. Previous investigations by [Benne and Homan, 2008] have identified the transitional regime, where the Reynolds number falls in the order of magnitude of 10^3 as best suited in storage-coupled thermosyphon systems, for obtaining more nearly uniform outlet temperatures. The analysis presumed, however, that the flow losses were entirely contained in the flow restriction section. Velocity profiles and the resulting skin friction coefficients have been examined for each of the three sections to assess this simplification.

The pressure drops across the different sections of the tube have also been identified. The results provide insight for determining appropriate geometry for desired transient performance of the novel thermosyphon assembly, when coupled to the storage volume.

The restriction section is investigated first, for the various results of interest as mentined above. The flow restriction element is the component most critical to obtaining desired transient performance. The straightening section is investigated next, followed by the heater section. In the heater section, the skin friction coefficients prove to be effected by gravity thereby indicating a mixed convection regime.

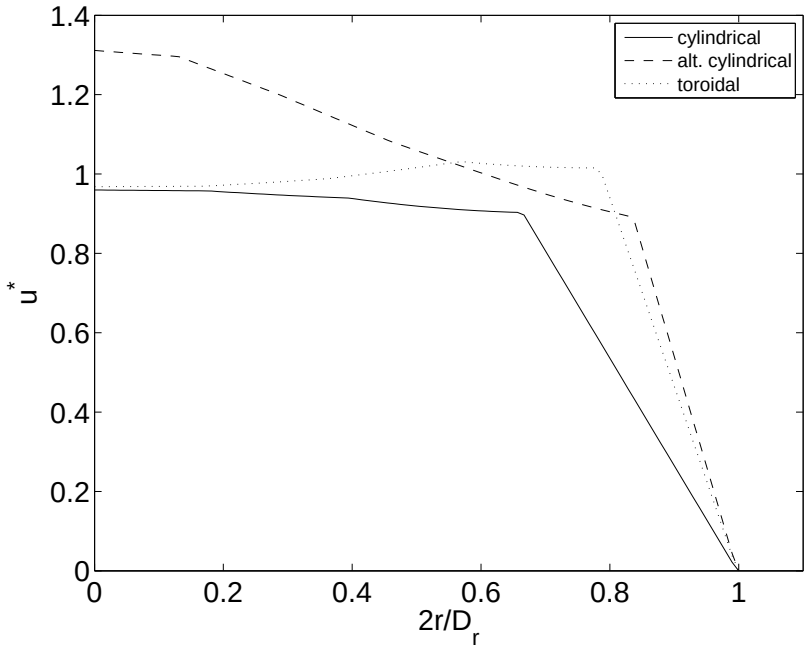

Figure 4.7. Velocity profiles at inlet to the flow restriction for $\dot{m} = 0.026$ kg/s. The Reynolds number in the restriction section for this case is Re $= 2710$. Numerical computations were carried out using the molecular viscosity model(laminar).

4.2.1. Flow Restriction Section. The flow restriction section is taken as six inches long, similar to that of the empirically tested assembly. The velocity profiles at the inlet to the restriction section have been plotted for mass flow inlet conditions of $\dot{m} = 0.026$ kg/s and 0.102 kg/s. Figure 4.7 and 4.8 show the velocity profiles at the two mass flow rates respectively. The flat velocty profile seen in the plots is due to the the sudden change in geometry from the straightening section with a diameter of $D_s = 1.5$ inches, to the restriction section which has a diameter $D_r = 0.5$ inch. The Reynolds number, at the entrance to restriction section is Re $= 2710$, when the mass flow rate, $\dot{m} = 0.026$ kg/s and Re $= 10200$ when the mass flow rate is $\dot{m} = 0.102$ kg/sec. Thus, at the low flow rate, the flow is just inside the laminar regime within the flow restriction. However at the high flow rate, the flow

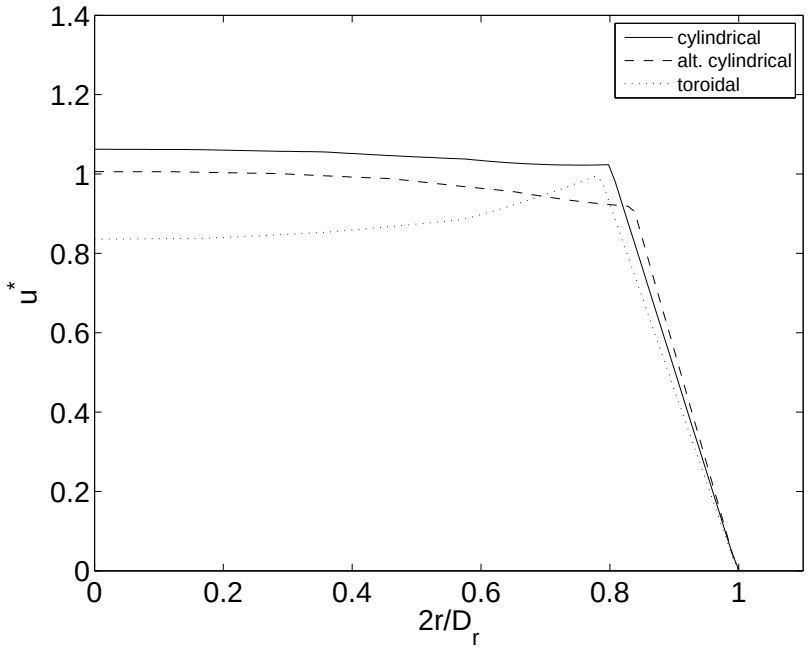

Figure 4.8. Velocity profiles at inlet to the flow restriction for $\dot{m} = 0.102$ kg/s. The Reynolds number in the restriction section for this case is Re $= 10200$. Numerical computations were carried out using the Standard K-ω turbulence viscosity model.

regime in the restriction section is fully turbulent. Flow development inside the restriction section is revealed by velocity profiles plotted at equal distances along the length of the flow restriction. The velocity profiles at low and high flow rates are shown in Figure 4.9 and 4.10 resectively. The velocity profiles inside the restriction element do not appear to be substantially developing, indicating fully developed flow.

The skin friction coefficient in the $D_r = 0.5$ inch restriction, for a fully developed flow at a mass flow rate of $\dot{m} = 0.026$ kg/s and Re $= 2170$ is given by the expression

$$C_f = \frac{64}{Re} \tag{4.1}$$

At this flow rate, $C_f = 0.029$. At a mass flow rate of $\dot{m} = 0.102$ kg/s and Re $= 10200$, the

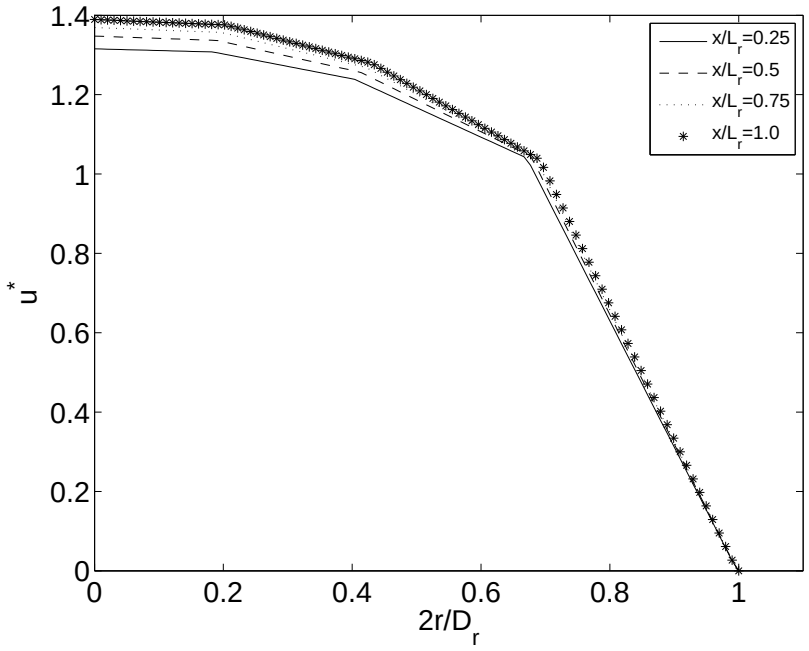

Figure 4.9. Velocity profiles at equal distances along the flow restriction for $\dot{m} = 0.026$ kg/s. The velocity profiles show very little development, indicating that the flow is fully developed. The heater geometry is cylindrical.

skin friction coefficient, given by the Blasius relation

$$C_f = \frac{0.079}{Re^{\frac{1}{4}}} \tag{4.2}$$

is 0.00786. Similarly, for the $D_r = 0.375$ inch flow restriction, fully developed skin friction coefficients are 0.0201 and 0.0075. Whereas, for $Dr = 0.625$ inch flow restriction, fully developed skin friction coefficients are 0.031 and 0.00821. Figure 4.11 shows the skin friction coefficient for varying D_r at a mass flow rate of 0.026 kg/s. The values obtained from ANSYS FLUENT indicate the skin friction coefficients are asymptoting to a constant value, indicating the flow could be fully developed inside the restriction. Figure 4.12 shows the skin friction cofficient at varying D_r at $\dot{m} = 0.102$ kg/s. The value of the skin friction

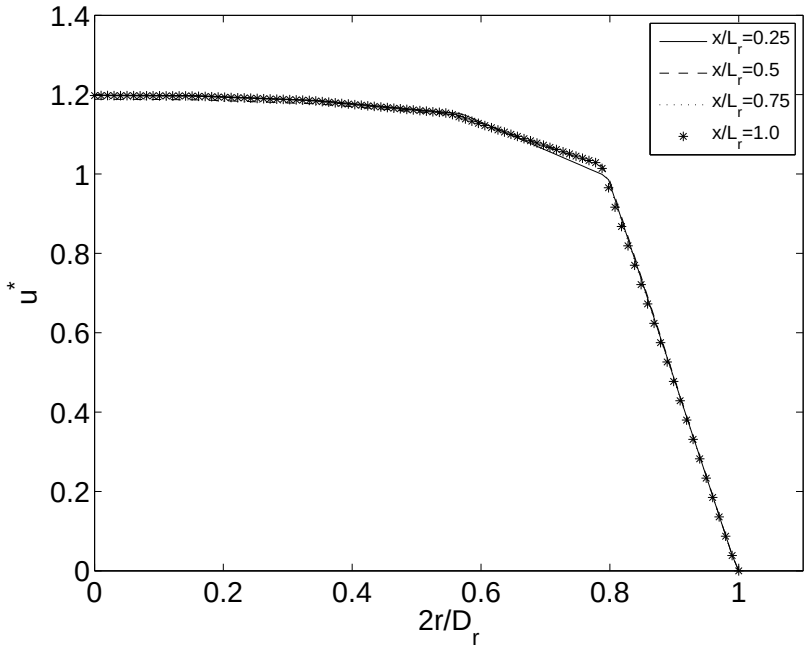

Figure 4.10. Velocity profiles at equal distances along the flow restriction for $\dot{m} = 0.102$ kg/s. The velocity profiles indicate that the flow is fully developed. The heater geometry is cylindrical.

coefficients is again sen to asymptote to a constant value.

There are differences in the values of the skin friction cofficient obtained analytically and numerically for both low and high-flow conditions. Although the Reynolds number obtained suggests that the low-flow and high-flow conditions correspond to flow in the laminar and turbulent regimes, there could be transitional flow in certain portions of the restriction. Transitional flow could lead to instabilities in the numerical solution due to their inherent complexity. The entrance length for $D_r = 0.5$ inch at low flow conditions is 81.3 inches, for $D_r = 0.375$ inch it is 71.3 inches and for $D_r = 0.625$ inch it is 76.5 inches. However with the length of the restriction section being only 6 inches, indications of a fully developed flow can be attributed to the use of a highly simplified model to study a

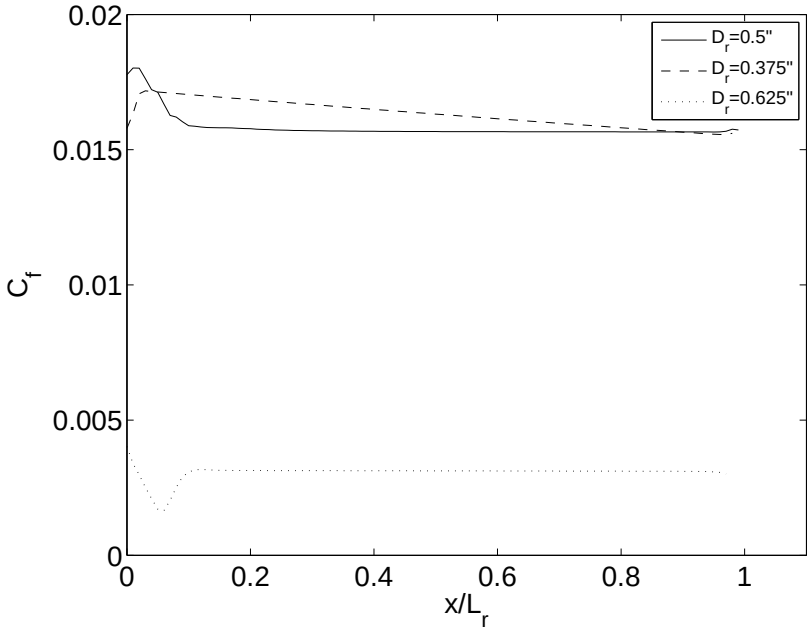

Figure 4.11. Skin friction coefficient in the flow restriction section for $D_r = 0.5$ inch, $D_r = 0.375$ inch and $D_r = 0.625$ inch flow restriction elements, with cylindrical heater for $\dot{m} = 0.026$ kg/s. The Reynolds number in the restriction section is 2170, 3170 and 2040 respectively. Numerical computations were carried out using the molecular viscosity (laminar) model.

transitional flow regime generated in the flow restriction. A simplified model such as the one used here may not be able to effectively capture the effects of a transitional flow in the flow restriction element.

The skin friction coefficient is also plotted for a $D_r = 0.5$ inch flow restriction with varying surface roughness. The mass flow rate is $\dot{m} = 0.102$ kg/s and Re $= 9170$. The skin friction coefficient for a fully developed flow in a rough pipe is determined analytically by the Colebrook equation given by

$$\frac{1}{\sqrt{f}} = -2.0log(\frac{1}{3.7D_r} + \frac{2.51}{Re\sqrt{f}}) \tag{4.3}$$

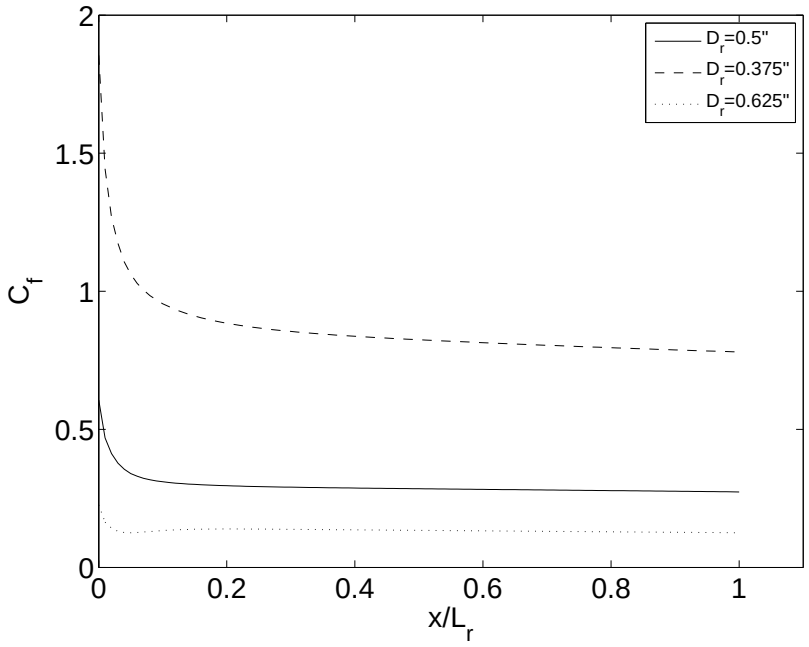

Figure 4.12. Skin friction coefficient in the flow restriction section for $D_r = 0.5$ inch, $D_r = 0.375$ inch and $D_r = 0.625$ inch flow restriction elements, with cylindrical heater for $\dot{m} = 0.102 kg/s$. The Reynolds number in the restriction section is 10200, 12300 and 8170 respectively. Numerical computations were carried out using the Standard K-ω turbulence viscosity model.

the skin friction coefficent for $k_s/D_r = 0.002$ is 0.034, for a $k_s/D_r = 0.01$, the skin friction coefficient is 0.043 and for $k_s/D_r = 0.05$, the skin friction coefficient is 0.073. Figure 4.13 shows the skin friction coefficient for varying roughness in the restriction section. There are differences between the values of the skin friction coefficient predicted numerically and those obtained analytically. One possible reason can be attributed to the number of elements in the restriction section. Grid resolution was carried out by comparing the numerical values of the skin friction coefficient in the straightening section against analytical values. Although the number of elements is maintained at 25000, the distribution of elemennts in the restrication is possibly not sufficient to obtain accurate results. There is also the

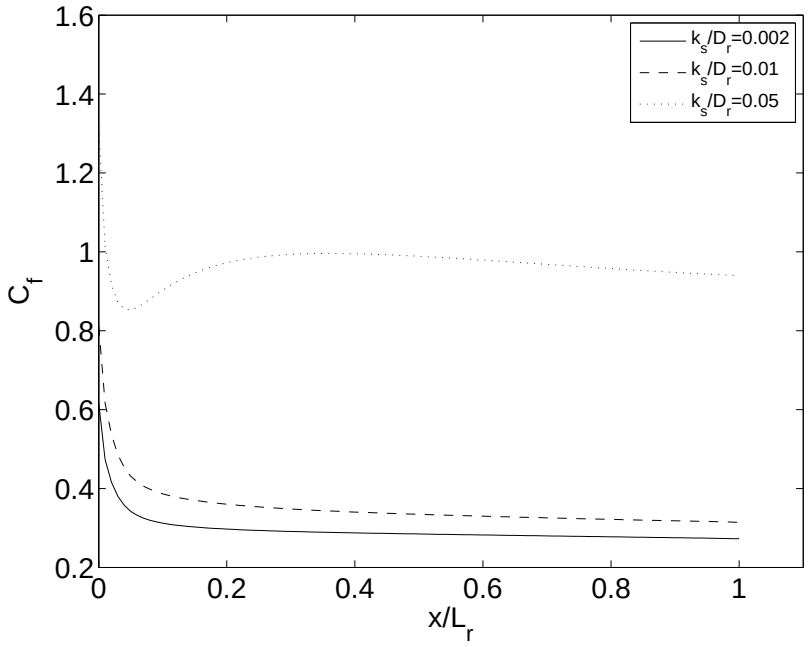

Figure 4.13. Skin friction coefficient in the flow restriction section for varying surface roughness given by $k_s/D_r = 0.002$, $K_s/D_r = 0.01$ and $k_s/D_r = 0.05$, with cylindrical heater for $\dot{m} = 0.102$ kg/s. The Reynolds number in the restriction section is 9170 respectively. Numerical computations were carried out using the Standard K-ω turbulence viscosity model.

possibility of the flow regime being transitional which could lead to uncertainities in the results.

4.2.2. Straightening Section. In the straightening section the diamter $D_s = 1.5$ inches. At a mass flow rate of $\dot{m} = 0.026$ kg/s, the value of the Reynolds number is only 934, well below the often used boundary of 2300 between laminar and turbulent regimes. Figure 4.14 shows the velocity profiles at the inlet to the straightening section for different heater gometries. For all the three heater geometries, it can be seen that the flow is developing at the inlet to the straightening section. The cylindrical and alternate cylindrical velocity profiles show similar velocity profiles, with the alternate cylindrical heater's velocity peaking at a slightly

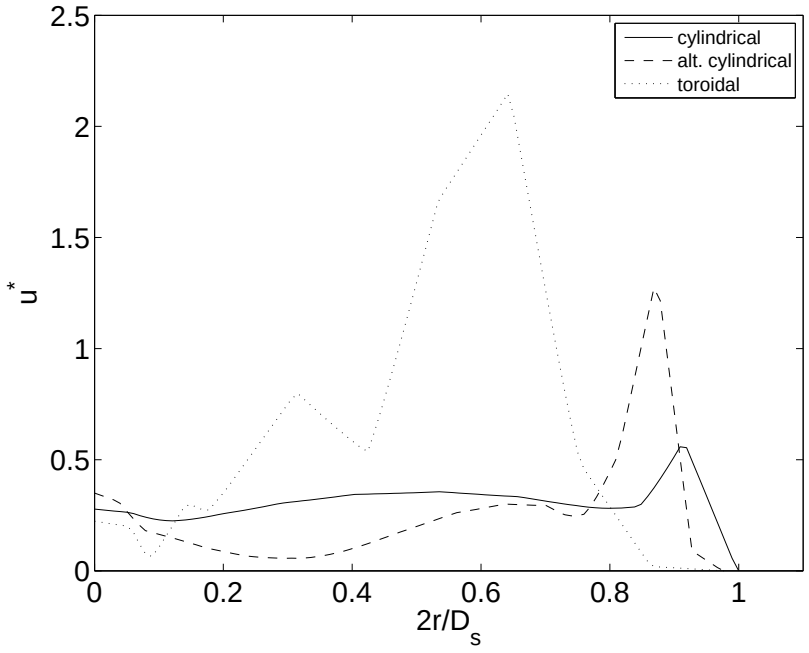

Figure 4.14. Velocity profiles at inlet to the straightening section for $\dot{m} = 0.026$ kg/s. The Reynolds number in the restriction section for this case is Re $= 934$. Numerical computations were carried out using the molecular viscosity model.

higher value than the cylnidrical heater. The peaks appear at an approximate location of 0.90 corresponding to the x coordinate for the cylindrical heater and at an approximate location of 0.875 for the alternate cylindrical heater. The coordinates correspond to the space between the heater wall and the thermosyphon wall, where the fluid flows. The toroidal heater has a different profile as compared to the two cylindrical heaters. The toroidal heater has a peak at an *x* coordfinate location of 0.6, this corresponds to the plume produced by the heating rings along the center of the thermosyphon assembly.

Figure 4.15 shows the temperature profiles at the inlet to the straightening section for the three different heater geometries. The temperature profiles for the cylindrical and alternate cylindrical heater have their peak at an *x* coordinate location of 0.82 and 0.90,

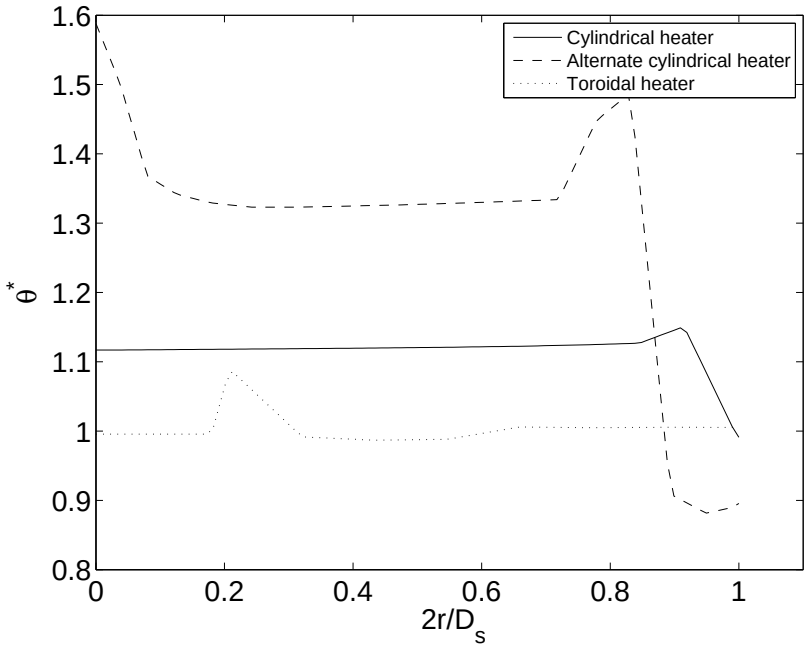

Figure 4.15. Temperature profiles at inlet to the straightening section for a $\dot{m} = 0.026$ kg/s. Peaks in the graph correspond to approximate flow passage locations occuring between the heater and the thermosyphon wall.

corresponding to the flow passage between the heater and the thermosyphon wall.

Velocity profiles at the inlet to the straightening section for the high flow rate of $\dot{m} = 0.102$ kg/s an Reynolds number Re $= 3700$ shows developing flow at the inlet to the straightening section. Figure 4.16 shows the velocity profiles at the inlet to the straightening section when $\dot{m} = 0.102$ kg/s. The toroidal heater in this case, has a much flatter profile compared to the previous case. This is due to the dissipation arising from the higher flow rate of 0.102 kg/s. Figure 4.17 shows the temperature profiles at inlet to the straightening section . The toroidal heater shows a flat temperature profile as compared to the other heater configurations. To understand how the flow develops along the length of the straightening section, velocity profiles are drawn at equidistant locations along the length of the tube.

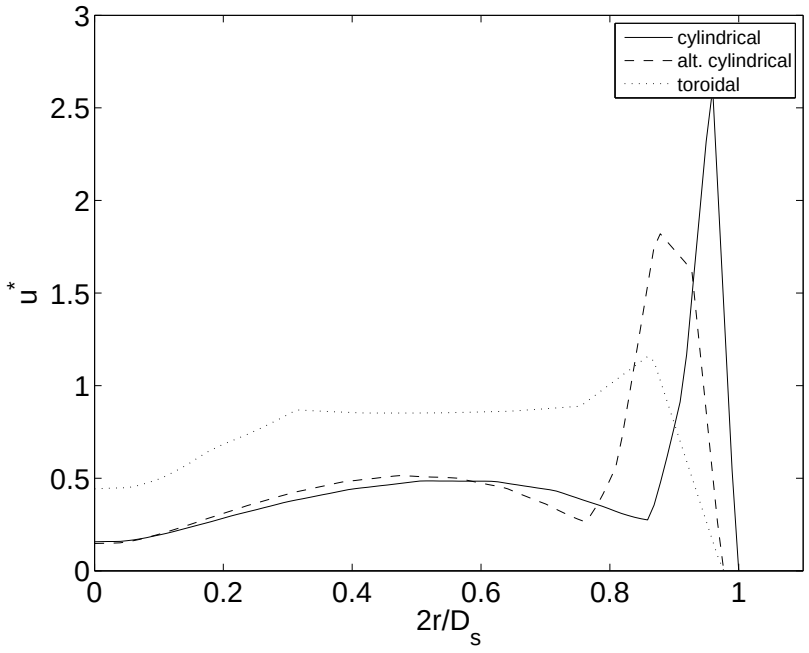

Figure 4.16. Velocity profiles at inlet to the straightening section for $\dot{m} = 0.102$ kg/s. The Reynolds number in the restriction section for this case is Re $= 3700$. Numerical computations were carried out using the STD K-ω turbulence viscosity model.

Figure 4.18 shows the velocity profiles in the straightening section for a mass flow rate of 0.026 kg/s. There is very little variation in the velocity profiles plotted along the length of the straightening section , indicating that the flow is fully developed. Figure 4.19 shows the temperature profiles for laminar flow condition in the straightening section. It is seen that the temperature in straightening section of the tube becomes uniform downstream of the heater. Figure 4.20 and 4.21 show the velocity and temperature profiles for a mass flow rate of 0.102 kg/s. The shape of the velocity profile does not change beyond $x/Ls = 0.25$, indicating that the flow is fully developed. The temperature profile indicates that there is uniform temperature in the tube similiar to the condition when the mass flow rate is 0.026 kg/s.

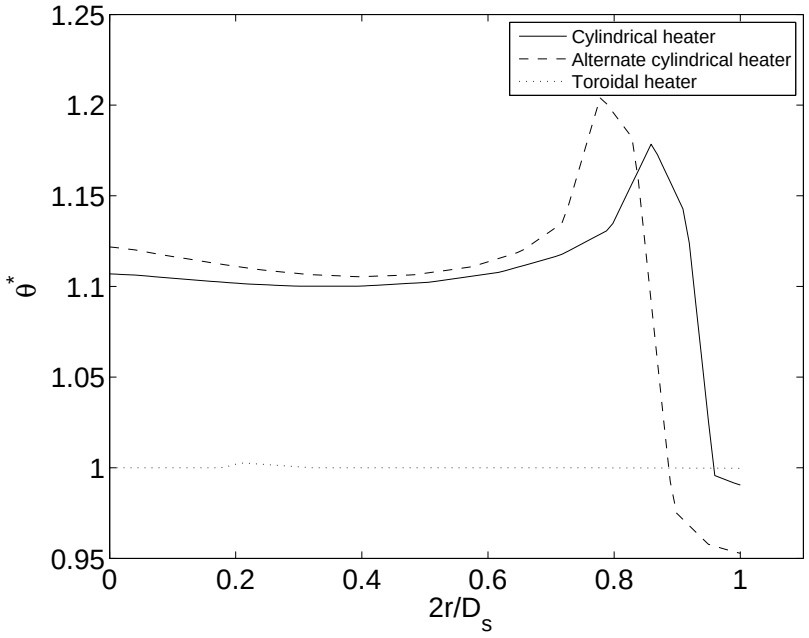

Figure 4.17. Temperature profiles at inlet to the straightening section for $\dot{m} = 0.102$ kg/s. Peaks in the graph correspond to approximate flow passage locations occuring between the heater and the thermosyphon wall.

The skin friction coefficient is computed analytically for a fully developed flow in the straightening section, using the Darcy friction factor, given by:

$$C_f = \frac{64}{R_e} \tag{4.4}$$

When $\dot{m} = 0.026$ kg/s, Re $= 934$ the skin friction coeficient $C_f = 0.068$. However when $\dot{m} = 0.102$ kg/s, the corresponding Reynolds number, Re is 3700, a value above the usual 2300 demarcation. The skin friction coefficient for turbulent fully develped flow in the straightening section is then once again determined by the Blasius relation and $C_f = 0.010$. The skin friction coefficient, C_f, is also computed numerically in ANSYS FLUENT and is plotted at the two different mass flow rates of 0.026 kg/s and 0.102 kg/s as shown in

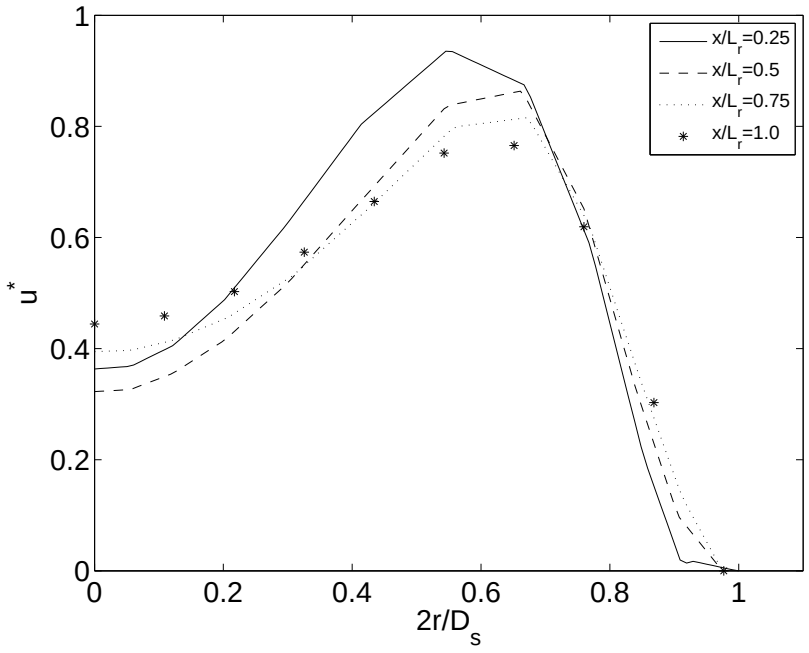

Figure 4.18. Velocity profiles at equal distances along the length of the straightening section for $\dot{m} = 0.026$ kg/s. The velocity profiles indicate that the flow is fully developed. The heater geometry is cylindrical. Numerical computations were carried out using the molecular viscosity model.

Figure 4.22 . The value of skin friction coefficient asymptotes to a constant value in the straightening section for both mass flow rate conditions. A difference between the values computed analytically and that obtained numerically from FLUENT when the mass flow rate is 0.026 kg/s is noted in the graph. The value of the skin friction coefficient using the Standard k-ω model yields values similar to analytical results. The velocity profile plots in the straightening section indicate that the flow is fully developed. The analytical values for the entrance length indicate 84.6 inches and 17.3 inches for the low and high mass flow rates respectively. The discrepency in the skin friction coefficient at a low mass flow condition can be due to the flow actually developing in the straightening section, rather than being fully devloped.

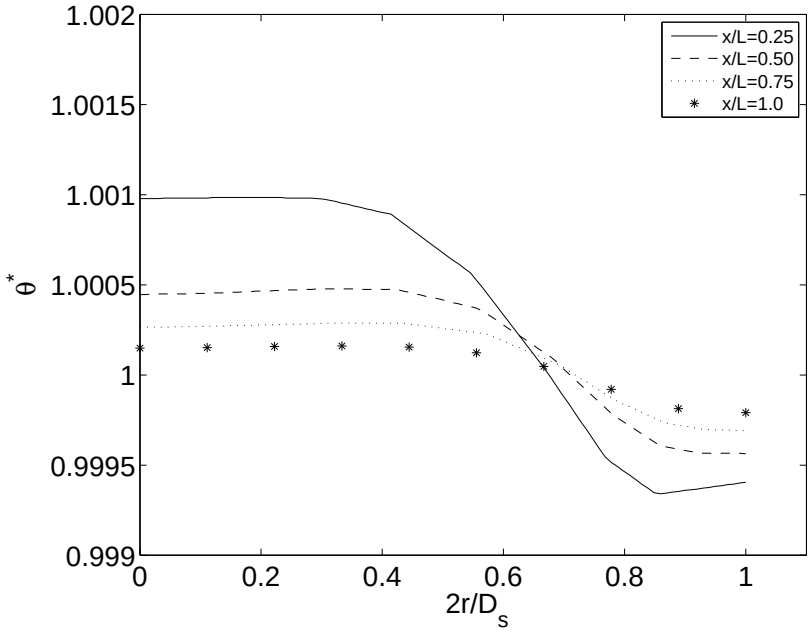

Figure 4.19. Temperature profiles along the length of the straightening section for $\dot{m} = 0.026$ kg/s. The temperature profiles indicate uniform temperature inside the thermosyphon tube assembly. Numerical computations were carried out using the molecular viscosity model.

4.2.3. Heater Section. In the heater section, a large constant heat flux is imposed as a thermal boundary condition. Since gravity acts in the downward direction, the heat addition causes an increase in the velocity of the fluid close to the heater and leads to mixed convection as described in [Metais and Eckert, 1964]. The mixed convection condition is one in which the velocity field is impacted by the heat transfer. Figure 4.23 shows that for Reynols number in the order of 10^3 and with sufficiently large Grashof numbers, which is the ratio of bouyancy forces to the viscous forces acting on a fluid, heat transfer regime in the fluid is in the mixed convection regime.

For the cylindrical heater configuration, with a mass flow rate of 0.026 kg/s, the Reynold's number Re $= 10600$. The skin friction coefficient for a fully developed flow

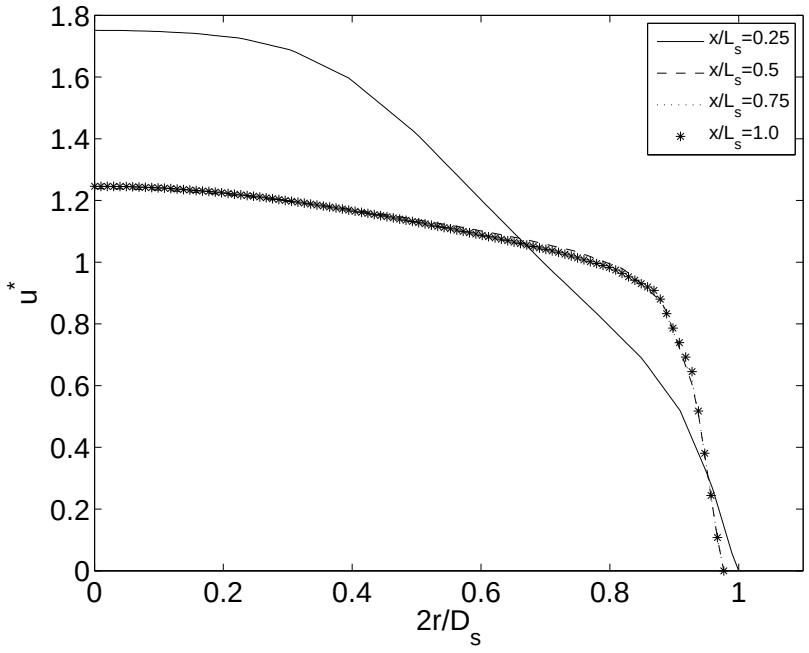

Figure 4.20. Velocity profiles at equal distances along the length of the straightening section for $\dot{m} = 0.102$ kg/s. The velocity profiles indicate that the flow is fully developed. The heater geometry is cylindrical. Numerical computations were carried out using the Standard K-ω turbulence viscosity model.

under these conditions, given by the Blasius relation is 0.0077. When the mass flow rate is 0.102 kg/s, the Reynolds number Re = 41700. The skin friction coefficient for a fully developed flow under these conditions, given by the Blasuis relation, is 0.0055. From Figure 4.24 and 4.25 , it is seen that the numerically computed skin friction coefficients tend to asymptote to a constant value. Difference between the analytical and numerical values of skin friction coefficients is noticed in the heater section. Although the cylindrical heater has high fluid velocities, the effect of gravity acting on the fluid, coupled with a large amount of heat flux imposed can lead to partial mixed convection in this section. It is known from previous investigations that in a mixed convection regime, there can be orders of magnitude differences when computing the skin friction coefficent. The differences in

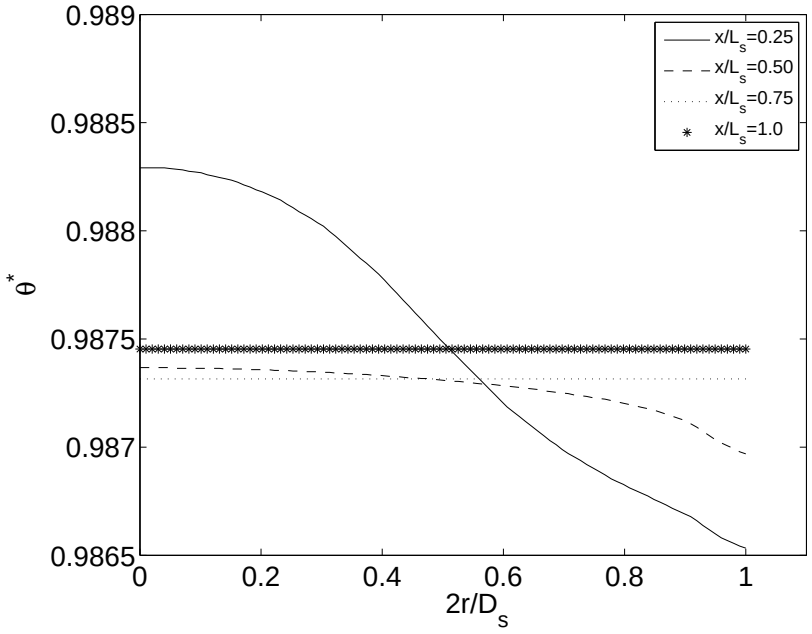

Figure 4.21. Temperature profiles along the length of the straightening section for $\dot{m} = 0.102$ kg/s. The temperature profiles indicate uniform temperature inside the thermosyphon tube assembly. Numerical computations were carried out using the Standard K-ω turbulence viscosity model.

the values can also be due to lesser mesh elements in the heater section as compared to the straightening section. Also the use of a simplified model makes it difficult to precisely predict behavior of a flow that exhibits mixed convection regime.

For the alternate cylindrical heater configuration the Reynolds number $\mathrm{Re} = 5200$ at a mass flow rate of $\dot{m} = 0.026$ kg/s. The skin friction coefficient for a fully developed flow is given by the Blasius relation is 0.010. With $\dot{m} = 0.102$ kg/s the Reynolds number $\mathrm{Re} = 20400$. The skin friction coefficient for a fully developed flow, given by the Blasius relation is 0.0066. Figures 4.26 and 4.27 show the plot of the skin friction coefficent for an alternate cylindrical heater. The numerically computed values do not asymptote to a constant value, this can be due to developing flow in the heater section. There is also a

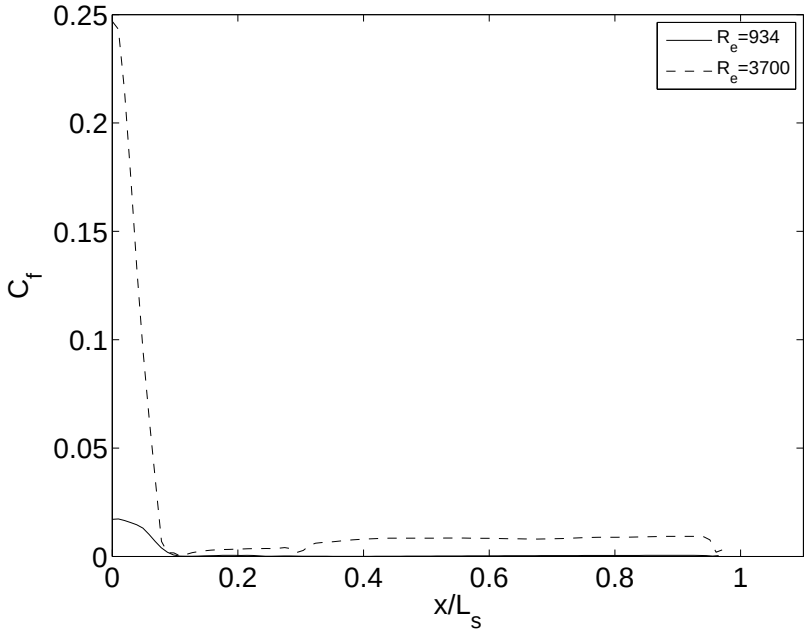

Figure 4.22. Skin friction coefficients in the straightening section for $\dot{m} = 0.026$ kg/s with Re $= 934$ and $\dot{m} = 0.102$ kg/s with Re $= 3700$. The skin friction coefficents asymptote to a constant value indicating that the flow is fully developed.

difference between analytically computed values and the numerical values. The difference can again be attributed to a lower number of mesh elements in the heater section and also estimating the skin friction coefficient effectively becomes difficults in the mixed convection regime.

In the toroidal heater configuration, with a mass flow rate, $\dot{m} = 0.026$ kg/s, the Re $= 1440$. The Skin friction coefficient for a fully developed flow is given by the Darcy-Weisbach equation and is 0.044. With a mass flow rate of $\dot{m} = 0.102$ kg/s, Re $= 5660$. The skin friction coefficient for a fully developed flow, given by the Blasius relation is 0.010. Figure 4.28 and 4.29 show the plots of the skin friction coefficient for a toridal heater. The effect of gravity is most pronounced in this heater configuration at a mass flow rate of $\dot{m} = 0.026$ kg/s and is subject to mixed convection. Irregularities in skin friction plot can

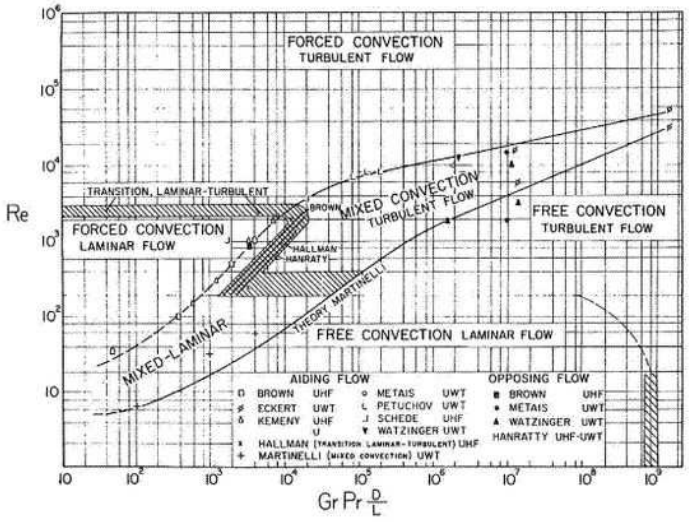

Figure 4.23. Mixed convection regime as shown in [Metais and Eckert, 1964]

be due to recirculation in the toroidal heater region. The skin friction plot shows peaks that correspond to the locations of the toroidal heaters in the thermosyphon assembly. The flow appears to be developing in the heater section.

4.2.4. Pressure Drops. The flow restriction plays a crucial role in determining the outlet temperature from the thermosyphon tube assembly. It is important to determine the percentage pressure drop that occurs across the flow restriction as compared to the overall pressure drop. Selecting the appropriate flow restriction is vital for designing the thermosyphon tube assembly that will yield optimal performance i.e. constant outlet temperature without varying the heat input.

Table 4.1 shows the ratio of the pressure drop across the flow restriction element to the overall pressure drop in the therosyphon tube for varying flow restriction diameters. For a 0.5 inch flow restriction, which gives the best experimental performance, it is seen that the pressure drop across flow restriction accounts for 37% of the total pressure drop. It is also

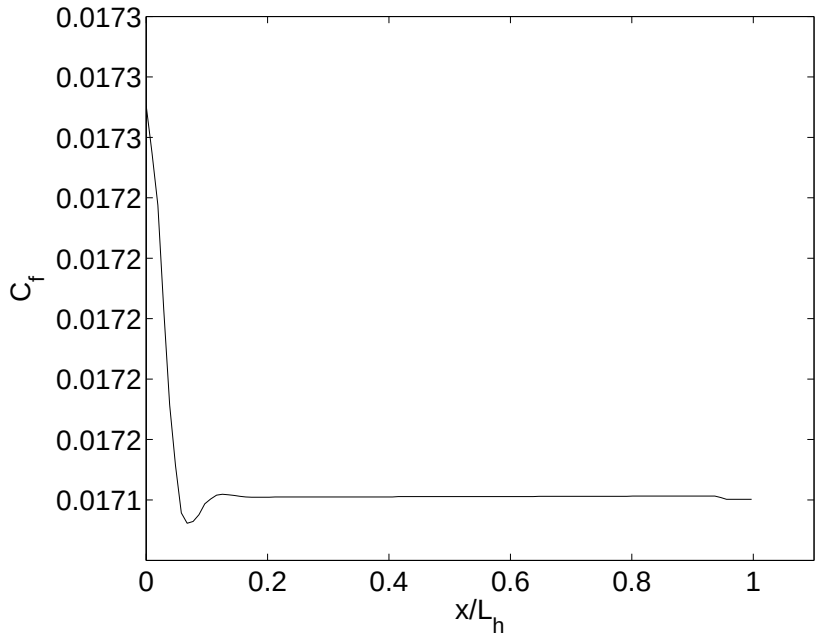

Figure 4.24. Skin friction coefficient for a cylindrical heater with $\dot{m} = 0.026$ kg/s. The Reynolds number Re $= 10600$ in the heater section. Numerical computations were carried out using the molecular viscosity (laminar) model.

seen that flow restrictions with diameters of 0.375in and 0.625 inch account for 46% and 17% respectively. However experimental testing for both these flow restriction diameters produce less than optimum performance. Table 4.2 shows the ratio of the pressure drop across a 0.5 inch flow restriction element to the total pressure drop for varying surface roughness. It is seen that as the roughness of the flow restriction element increases the percentage pressure drop across the flow restriction element also increases. From the above two tables it can be seen that in a real system, although considerable pressure drop occurs in the flow retriction section , not all of the pressure drop occurs there as presumed by [Benne and Homan, 2008]. Therefore to obtain optimum performance, care has to be taken when designing such a thermosyphon system, for use with finite reservoir such as the storage volume of the resistance heater.

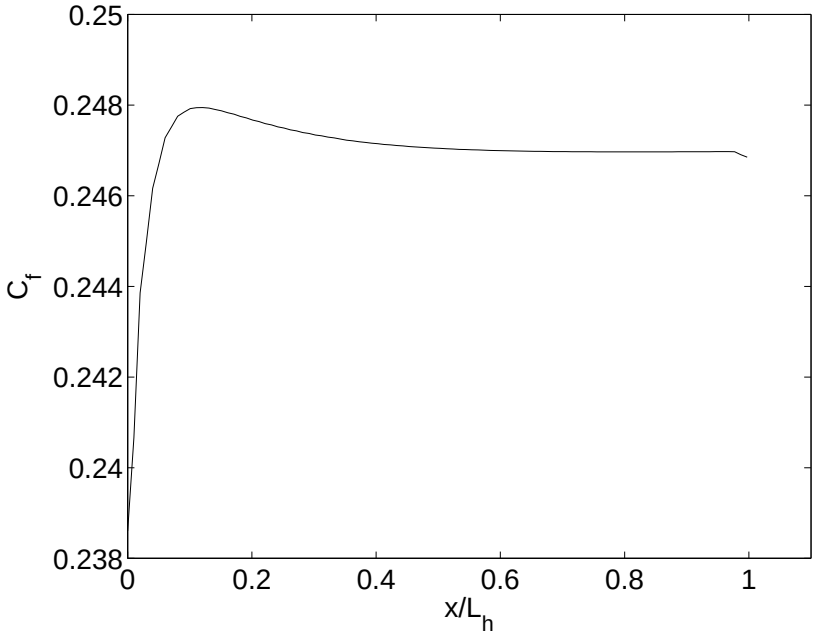

Figure 4.25. Skin friction coefficient for a cylindrical heater with $\dot{m} = 0.102$ kg/s. The Reynolds number Re $= 41700$in the heater section. Numerical computations were carried out using the Standard K-ω turbulence viscosity model.

4.2.5. Conclusion. Computational results indicate fully developed flow in the restriction and straightening sections of the thermosyphon assembly. The plots of the skin friction coefficient also asymptote to a constant value. Analytical results however, indicate differences between them and the values computed numerically. Also entrance lengths indicate that the flow should be developing in the restriction section. Differences in the computational and analytical results is due to simplified treatment of a complex problem involving a possible transition flow regime in the restriction section and mixed convection in the heater section. A more detailed model will be needed to better study the flow dynamics inside the thermosyphon assembly.

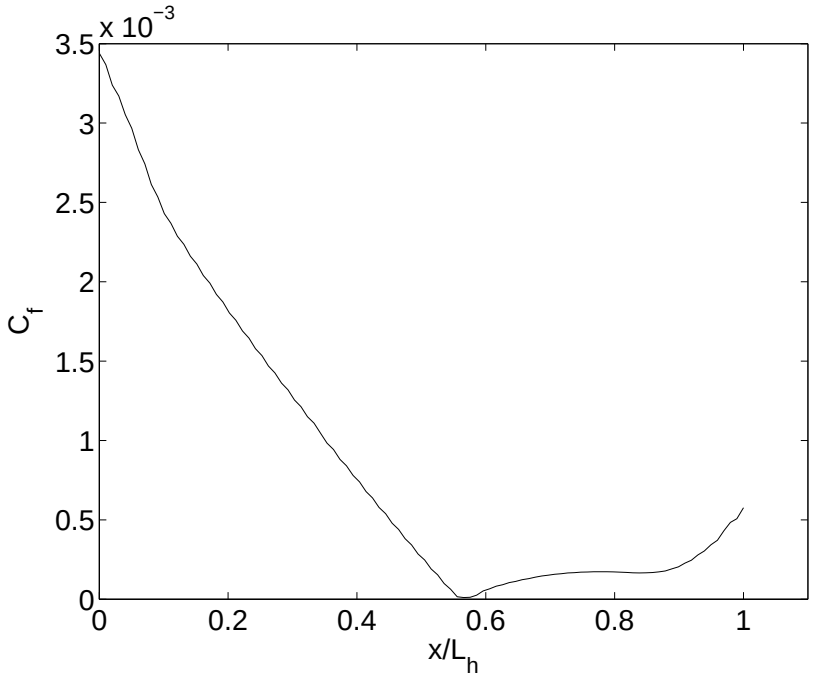

Figure 4.26. Skin friction coefficient for an alternate cylindrical heater with $\dot{m} = 0.026$ kg/s. The Reynolds number Re $= 5200$ in the heater. Numerical computations were carried out using the molecular viscosity (laminar) model.

Table 4.1. Ratio of pressure drop across the flow restriction element to the overall pressure drop for varying flow restriction diamters D_r.

D_r	$\Delta P_{FRE}/\Delta P_{OA}$
0.5 in	0.37
0.375 in	0.46
0.625 in	0.17

Table 4.2. Ratio of pressure drop across a 0.5 inch flow restriction element to the total pressure drop across thethermosyphon tube for varying flow restriction element roughness.

K_s/D_r	$\Delta P_{FRE}/\Delta P_{OA}$
0.002	0.37
0.01	0.39
0.05	0.44

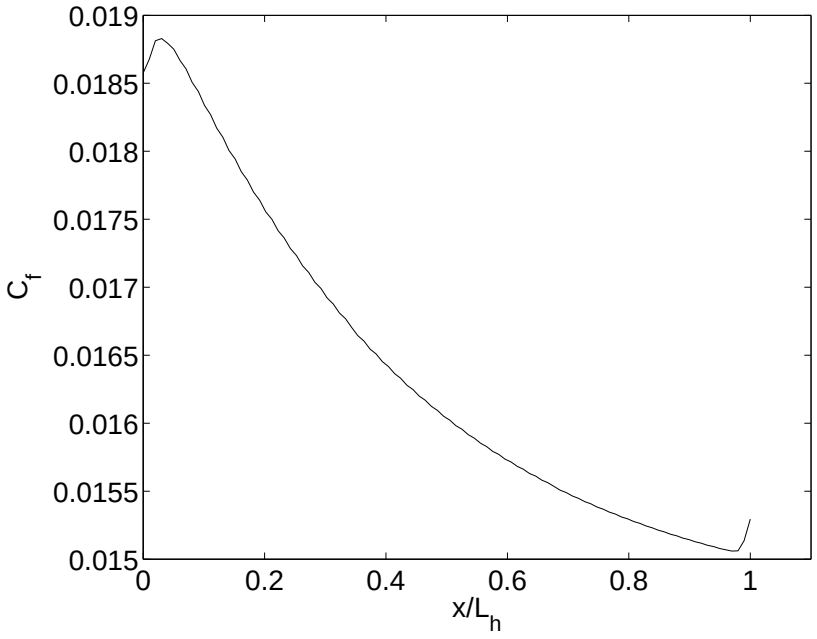

Figure 4.27. Skin friction coefficient for an alternate cylindrical heater with $\dot{m} = 0.102$ kg/s. The Reynolds number Re $= 20400$ in the heater section . Numerical computations were carried out using the STD K-ω turbulence viscosity model.

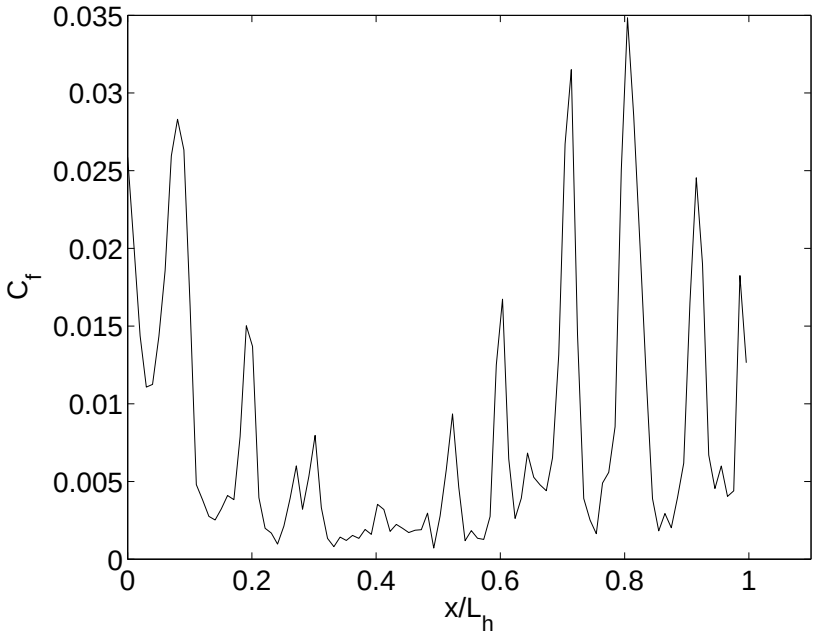

Figure 4.28. Skin friction coefficient for a toroidal heater with a mass flow rate of 0.026 kg/s. The Reynolds number $\mathrm{Re} = 1440$ in the heater section. Numerical computations were carried out using the molecular viscosity model.

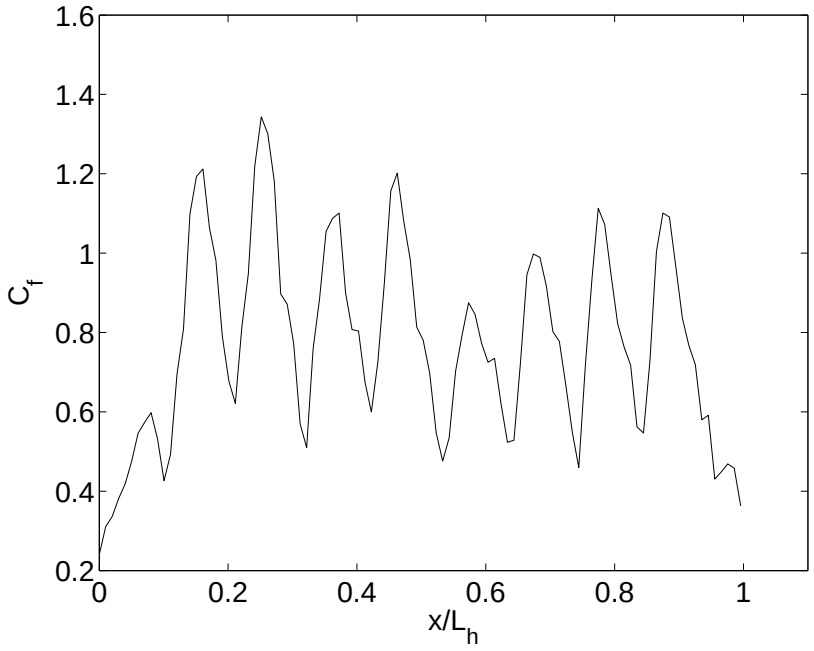

Figure 4.29. Skin friction coefficient for a toroidal heater with $\dot{m} = 0.102$ kg/s. The Reynolds number Re $= 5660$ in the heater section. Numerical computations were carried out using the STD K-ω turbulence viscosity model.

5. SUMMARY AND RECOMMENDATIONS

5.1. SUMMARY

This thesis studied the effects of coupling a thermosyphon tube assembly into a thermal storage device such as a resistance water heater. The water heater was tested for First Hour Ratings and Energy Factor Rating in both the conventional version and the modified version, operating with a thermosyphon tube assembly. From the results it is seen that the First Hour Rating is geometry sensitive, with the thermosyphon configuration yielding a significantly higher First Hour Rating. Isolating the heat addition surfaces, as in the thermosyphon configuration, prevented loss of thermal stratification. This resulted in an increase in the First Hour Rating of the modified water heater. Experimentally a 0.5 inch flow restriction element in the thermosyphon assembly resulted in optimum outlet water temperature from the thermosyphon assembly. A smaller flow restriction of 0.375 inch resulted in excessively high outlet temperatures from the thermosyphon tube. Whereas a larger flow restriction of 0.625 inch resulted in an outlet temperature too low for typical requirements.

Energy Factor Ratings for all three configurations yielded similar results which indicates that the Energy Factor is independant of the internal geometry. The energy factor is controlled by the level of insulation surrounding the system.

Computaions carried out on the thermosyphon tube assembly indicated that a large amount of pressure drop occurs across the flow restriction element although significant pressure drop may also occur in the heater section, where mixed convection is dominant. However, a thermosyphon tube can be designed in such a way that the dominant frictional losses occur across the flow restriction element. The computational prediction of skin

friction coefficients, indicates that the flow is fully developed in the restriction and straightening sections of the thermosyphon assembly. However, there is a difference between the skin friction coefficients computed analytically and that obtained numerically. The differences occur due to lesser grid resolution in the heater and restriction sections. There is also a possibility of transitional flow in the restriction section and mixed convection in the heater section, which could affect the accuracy of a simplified model such as the one used in this investigation. The velocity profiles in the restriction and straightening sections also indicate fully developed flow, however analytical calculations of the development length indicate that the flows should still be devloping in them. This can again be due to lesser number of grid elements in these sections.

In conclusion, operating the water heater in the thermosyphon configuration results in higher First Hour Rating due to a small amount of unmixed hot water that is available from the outlet of the thermosyphon tube, leading to better stratification and therefore improved thermal performance of the resistance storage water heater. Computations carried out give an insight into the complex flow dynamics of the thermosyphon assembly and warrant a more complex model to study the same.

5.2. RECOMMENDATIONS FOR FUTURE RESEARCH.

- There is need for better inlet temperature control of water into the heater.
- Better insulation of the piping system in the experimental setup will reult in more accurate energy factor results.
- Installing the thermosyphon assembly in a different capacity heater, to see the effect on the performance.
- A comprehensive 3D model of the thermosyphon assembly is needed to get better

insight into the flow dynamics of the assembly.

- A comprehensive model is needed to design the flow restriction diameter of the thermosyphon assembly.

BIBLIOGRAPHY

KS Benne and KO Homan. Dynamics of a closed-loop thermosyphon incorporating thermal storage. *Numerical Heat Transfer, Part A: Applications*, 54(3):235–254, 2008.

Kyle S Benne and KO Homan. Transient behavior of thermosyphon-coupled sensible storage with constant temperature heat addition. *Numerical Heat Transfer, Part A: Applications*, 55(2):101–123, 2009.

José Fernández-Seara, Jaime Sieres, et al. Experimental analysis of a domestic electric hot water storage tank. part ii: dynamic mode of operation. *Applied thermal engineering*, 27(1):137–144, 2007.

Adel A Hegazy. Effect of inlet design on the performance of storage-type domestic electrical water heaters. *Applied Energy*, 84(12):1338–1355, 2007.

Adel A Hegazy and MR Diab. Performance of an improved design for storage-type domestic electrical water-heaters. *Applied energy*, 71(4):287–306, 2002.

Kelly O Homan. Internal small volume storage water heater, October 3 2006. US Patent 7,114,468.

A Kerim Kar and Ümit Kar. Optimum design and selection of residential storage-type electric water heaters for energy conservation. *Energy conversion and management*, 37 (9):1445–1452, 1996.

JW McMenamy and KO Homan. Transient and rate-dependent performance of conventional electric storage water heating systems. *Journal of solar energy engineering*, 128 (1):90–97, 2006.

B Metais and ERG Eckert. Forced, mixed, and free convection regimes. *Journal of Heat Transfer*, 86(2):295–296, 1964.

KE Torrance. Open-loop thermosyphons with geological applications. *Journal of Heat Transfer*, 101(4):677–683, 1979.

VITA

Siddarth Ashokkumar was born in Madras (now Chennai), Tamil Nadu on July 26th, 1987. In May 2005, he graduated from St.Michael's Academy Higher Secondary School. In fall 2005, he joined the undergraduate program in Marine Engineering at Birla Institue of Technology and Science, Pilani, Rajasthan. He graduate with a Bachelor of Science degree in Marine Engineering in fall 2009. Upon graduation, he joined a shipping company in India as a sea going trainee Engineer. He then rose through the ranks to become an officer in the Indian Merchant Navy.

In fall 2012, he enrolled for a master's degree in Mechanical Engineering at Missouri University of Science and Technology. At Missouri S&T, he carried out research work under the guidance of Dr. Kelly Homan, on thermosyphon based water heaters. He also served as Treasurer for India Association and photographer for the Interntaional Students Club at Missouri S&T. He graduated with a Master of Science in Mechanical Engineering from Missouri University of Scienc and Technology in May 2015.